Iron mineralogy across the oxycline of a lignite mine lake

Jennyfer Miot, Shipeng Lu, Guillaume Morin, Areej Adra, Karim Benzerara, Kirsten Küsel

▶ **To cite this version:**

Jennyfer Miot, Shipeng Lu, Guillaume Morin, Areej Adra, Karim Benzerara, et al.. Iron mineralogy across the oxycline of a lignite mine lake. Chemical Geology, 2016, 434, pp.28-42. 10.1016/j.chemgeo.2016.04.013 . hal-01307099

HAL Id: hal-01307099

https://hal.sorbonne-universite.fr/hal-01307099

Submitted on 26 Apr 2016

HAL is a multi-disciplinary open access archive for the deposit and dissemination of scientific research documents, whether they are published or not. The documents may come from teaching and research institutions in France or abroad, or from public or private research centers.

L'archive ouverte pluridisciplinaire **HAL**, est destinée au dépôt et à la diffusion de documents scientifiques de niveau recherche, publiés ou non, émanant des établissements d'enseignement et de recherche français ou étrangers, des laboratoires publics ou privés.

ACCEPTED MANUSCRIPT

Iron mineralogy across the oxycline of a lignite mine lake

Jennyfer Miot[1*], Shipeng Lu[2,3,4], Guillaume Morin[1], Areej Adra[1], Karim Benzerara[1], Kirsten Küsel[2,3]

[1] Institut de Minéralogie, Physique des Matériaux et Cosmochimie (IMPMC). Muséum National d'Histoire Naturelle, Université Pierre et Marie Curie, Sorbonne Universités, Centre National de la Recherche Scientifique UMR 7590, IRD 206. 4 place Jussieu, 75 005 Paris, France.

[2] Institute of Ecology, Friedrich Schiller University Jena, Jena, Germany.

[3] The German Centre for Integrative Biodiversity Research (iDiv) Halle-Jena-Leipzig, Leipzig, Germany.

[4] Present address: Department of Chemical and Biological Engineering, Center for Biofilm Engineering, Montana State University, Bozeman, USA.

* Corresponding author: jmiot@mnhn.fr

ACCEPTED MANUSCRIPT

ACCEPTED MANUSCRIPT

Abstract

Iron-rich pelagic aggregates of microbial origin named "iron snow" are formed in the water column of some acidic lignite mine lakes. We investigated the evolution of Fe mineralogy across the oxycline of the Lusatian lake 77, Germany at two sampling sites differing by their pH and mixing profiles. The central basin (CB) of this lake shows a dimictic water regime with a non-permanent anoxic deep layer and a homogeneous acidic pH all over the water column (pH 3). In contrast, the northern basin (NB) is meromictic with a permanently anoxic bottom layer and a pH increase from pH 3 in the mixolimnion (superficial part of the lake) to pH 5.5 in the monimolimnion (anoxic bottom layer). Fe minerals above and below the oxycline were identified using X-ray Absorption Spectroscopy (XAS) at the Fe K-edge and further characterized down to the atomic scale by High Resolution Transmission Electron Microscopy (HRTEM) and Scanning Transmission Electron Microscopy (STEM) coupled to Energy Dispersive X-ray Spectroscopy (EDXS). We explored local Fe redox state and C speciation using Scanning Transmission X-ray Microscopy (STXM) at the Fe $L_{2,3}$-edges and C K-edge. Schwertmannite [$Fe_8O_8(OH)_{8-2x}(SO_4)_x$] identified as the sole Fe mineral in CB, was polycrystalline, consisting in the aggregation of nanodomains of 2-3 nm each one exhibiting the crystal structure of schwertmannite. In contrast, schwertmannite was partly (40%) converted to aluminous ferrihydrite when reaching the oxycline in NB. This mineralogical transformation was most probably due to a combination of abiotic and microbial anaerobic processes promoting pH increase and release of Fe(II) (e.g. via heterotrophic Fe(III) reduction) that induce the catalytic hydrolysis of schwertmannite to ferrihydrite. Mineral products were stabilized in the monimolimnion by the

ACCEPTED MANUSCRIPT

adsorption of aluminum, silicate and organic matter. Noteworthy, local Fe redox state heterogeneities were observed, with a few areas enriched in Fe(II) as evidenced by STXM analyses at the Fe $L_{2,3}$-edges. These local redox heterogeneities could arise from microbial activity (e.g. Fe(III) and/or sulfate reduction). All these results provide an in-depth mineralogical overview of iron phases forming in Lake 77 as a basis for future investigations of microbial vs. abiotic parameters controlling their stability and transformation.

Keywords: schwertmannite; mine lake; iron snow; STXM; HRTEM; iron reducing bacteria; biomineralization

ACCEPTED MANUSCRIPT

ACCEPTED MANUSCRIPT

1. Introduction

From early Earth to modern environments, oxidative weathering of Fe sulfides has been a major source of acidity and has supplied high amounts of dissolved sulfate and iron species to surface waters. This process was indeed active since the Archean, as suggested by the Cr isotope record around the Great Oxidation Event (Anbar et al., 2007; Crowe et al., 2013; Konhauser et al., 2011; Reinhard et al., 2013). Nowadays similar processes take place at acid rock or mine drainages (Lu and Wang, 2012) or in acidic lignite mine lakes (Blodau, 2006).

In such ferruginous environments, Fe(III) minerals precipitate massively. For instance iron oxyhydroxide and oxyhydroxysulfate precipitates are emblematic of acid rock drainages such as those located in the Iberian Pyrite Belt (Fernández-Remolar et al., 2005; Sánchez España et al., 2005). Another example of such iron mineralization occurs in acidic lignite mine lakes formed in former coal mine pits (Blodau, 2006; Küsel, 2003). They exhibit high rates of Fe(II) oxidation leading to massive precipitation of Fe(III)-bearing minerals, in the form of iron-rich aggregates termed “iron snow” (Reiche et al., 2011).

The nature of Fe-bearing phases occurring in such environments is strongly pH dependent. Schwertmannite [$Fe_8O_8(OH)_{8-2x}(SO_4)_x$; $1 \leq x \leq 1.75$] (Bigham et al., 1994) and/or jarosite [$(H, K, Na)Fe_3(OH)_6(SO_4)_2$)] are usually predominant under acidic conditions (pH 2.8-4.5) (Bigham et al., 1996), whereas at higher pH, ferrihydrite and/or goethite are more stable (Bigham et al., 1996; Gagliano et al., 2004; Sánchez-España et al., 2012, 2011). This diversity of Fe minerals plays a key role in controlling heavy metal(loid)s mobility (Burgos et al., 2012; Morin and Calas, 2006; Nordstrom, 2011). For instance, schwertmannite as well as mixed Fe and As oxyhydroxysulfates are known to

ACCEPTED MANUSCRIPT

efficiently scavenge arsenic in acid mine drainages (Carlson et al., 2002; Maillot et al., 2013; Morin et al., 2007, 2003). However the mechanisms controlling the precipitation and stability of these various mineral species are not fully understood. In particular, although the atomic structure of nanocrystalline schwertmannite has been elucidated using pair distribution function analysis (Fernandez-Martinez et al., 2010), the nanoscale structure (French et al., 2012; Hockridge et al., 2009), composition and stability (Caraballo et al., 2013; Regenspurg et al., 2004) of this phase remain a matter of debate.

Beyond abiotic factors (pH, redox potential, saturation state), microbial parameters contribute to the formation and/or stabilization of such Fe minerals. Many acidophilic Fe-cycling bacteria are part of the microbial diversity in these environments (Bonnefoy and Holmes, 2012; Johnson et al., 2012; Küsel, 2003) and retrieve energy from Fe(II) oxidation (Nordstrom and Southam, 1997). This leads to Fe minerals closely associated with microbial organic matter in acidic ferruginous environments (Benzerara et al., 2008; Clarke et al., 1997; Hedrich et al., 2011; Inskeep et al., 2004; Mori et al., 2015; Ohnuki et al., 2004) and in laboratory cultures (Egal et al., 2009; Liao et al., 2009; Morin et al., 2003; Sandy Jones et al., 2014; Xu et al., 2014; Zhu et al., 2013). Fe mineralogy may furthermore be modified through the activity of Fe(III)-reducing and sulfate-reducing microorganisms reported in such acidic environments (e.g. Bingjie et al., 2014).

Redox gradients are prone to the activity of such Fe cycling microbes and thus to Fe mineral (trans)formation. Whereas the oxycline is usually located within the sediment, this redox transition zone is present within the water column of some meromictic ferruginous lakes exhibiting either neutral (Crowe et al., 2008; Viollier et al., 1997) or acidic pH (Blodau, 2006; Reiche et al., 2011) that share analogies with early

ACCEPTED MANUSCRIPT

Earth environments (Busigny et al., 2014; Canfield et al., 2008). This oxycline is inhabited by a diversity of microbes involved in the Fe redox cycle (Crowe et al., 2008; Lehours et al., 2009, 2007, 2005; Lu et al., 2013, 2010; Walter et al., 2014), some of which are potentially involved in the biomineralization of Fe-bearing phases (Cosmidis et al., 2014; Llirós et al., 2015; Lu et al., 2013; Miot et al., 2016). Interplay of Fe(II)-oxidizing and Fe(III)-reducing bacteria might thus contribute to the control of Fe mineralogy.

Estimating the respective contributions of abiotic vs. microbial processes in controlling Fe mineralogy in redox transition zones remains a critical issue. As a first stage towards understanding these mechanisms, we performed an in-depth study of Fe mineralogy across the oxycline of a lignite mine lake (Lusatian Lake 77, Germany). This lake is characterized by an acidic pH and high dissolved Fe(II) (up to 12 mM in the bottom water) and sulfate (up to 30 mM) concentrations, arising from Fe sulfide oxidative weathering (Blodau, 2006; Küsel, 2003). It is composed of two basins: the northern basin (NB) is meromictic, i.e. permanently stratified with a deep anoxic layer (monimolimnion), whereas the central basin (CB) is dimictic, i.e. undergoes mixing in spring and autumn. A diversity of chemoautotrophic iron oxidizers and heterotrophic iron reducers have been identified as active players of the Fe biogeochemical cycle around the redoxcline of this lake (Lu et al., 2013). In the present study, we used X-ray absorption spectroscopy at the Fe K-edge to determine the nature of Fe minerals, including amorphous or poorly crystalline phases. In addition, we combined high resolution transmission electron microscopy (HRTEM) and synchrotron-based scanning transmission X-ray microscopy (STXM) to investigate the speciation of iron and associated organic matter down to the nanometer scale. Our results open a discussion of the stability of Fe minerals across the oxycline of Lake 77.

ACCEPTED MANUSCRIPT

2. Materials and Methods

2.1. Lake characteristics and sampling

The acidic lignite mine Lake 77 is located in the Lusatian mining area in east-central Germany and was formed after mining activity had stopped in 1960. The lake is composed of two basins: (a) the central basin (CB) exhibits a dimictic water regime with a full circulation of the water in spring and autumn and (b) the smaller meromictic northern basin (NB) has a deep permanently anoxic water body that is not influenced by lake circulation (Fleckenstein et al., 2009; Reiche et al., 2011). The bottom water of the NB has higher pH value, conductivity and dissolved Fe(II) and sulfate concentrations probably due to the inflow of less acidic contaminated groundwater (Fleckenstein et al., 2009; Neumann et al., 2013; Reiche et al., 2011). At each sampling time, pH, temperature, conductivity and dissolved oxygen content of the lake water were measured over depth with a multi-parameter probe (YSI Pro Plus, YSI, USA). The polarographic dissolved oxygen probe was calibrated with air-saturated water. The resolution for this probe is 0.01 $mg.L^{-1}$ and the accuracy 0.2 $mg.L^{-1}$ in the range 0-20 $mg.L^{-1}$. The pH-meter probe was calibrated by typical two-point calibration, using buffers at pH 4.0 and 7.0. The resolution of this probe is 0.01 units and the accuracy 0.2 units. The decline of the oxygen concentration marked the oxycline. To collect iron rich pelagic aggregates ("iron snow" particles) at different redox conditions, water samples were taken in November 2013 from 6-m depth at CB (after miximng of the CB) and from above, within and below the oxycline (4.5 m, 5.5 m and 6 m depth) at NB. In September 2014, water samples were taken before mixing of the CB from above, within and below

ACCEPTED MANUSCRIPT

the oxycline (5 m, 5.6 m and 6 m depth) and at NB from 4.3 m, 4.9 m and 6 m depth. Water samples were collected using a Ruttner water sampler and filled into bottles pre-flushed with nitrogen gas to avoid further oxygenation, sealed and transferred to laboratory in a cooling box. Bottles were opened in an anaerobic chamber (O_2< 0.2%) and iron snow particles were transferred to smaller bottles after sedimentation, then kept under cool conditions until further analyses. O_2 contamination is expected to remain limited given the methods used for sampling and given the slow kinetics of Fe(II) oxidation at the acidic pH of the lake water. For samples from NB (September 2014), concentrations of dissolved Fe(II) were measured spectrophotometrically using the phenanthroline method (Tamura et al., 1974). Sulfate concentration was measured turbidimetrically by the barium-chloride method (Tabatabai, 1974).

2.2. X-ray Absorption Spectroscopy

2.2.1. Sample preparation

For XAS analyses, samples from September 2014 exhibiting the highest content in particulate matter (CB-6.0m-2014, NB-4.9m-2014, NB-6.0m-2014) were prepared in an anoxic glovebox (pO_2 < 50 ppm). Water samples were centrifuged at 7000 *g* 15 min, then rinsed twice in deoxygenated mQ water (with pH adjusted at the lake water pH using HCl) and vacuum dried. The powder was gently grinded in an agate mortar and pressed as pellets in mixture with appropriate amount of cellulose in order to obtain absorption edge height ($\Delta\mu x$) as close as possible to one.

2.2.2. XAS data collection and analyses

ACCEPTED MANUSCRIPT

Fe K-edge XAS spectra of the lake samples were recorded at 77 K in transmission detection mode at the XAFS beamline (ELETTRA, Italy), using a Si(111) double-crystal monochromator. Energy was calibrated by setting to 7112 eV the first inflexion point of Fe-foil K-edge recorded in double-transmission setup. The spectra were merged and normalized using the Athena program (Ravel and Newville, 2005) and Extended X-ray Absorption Fine Structure (EXAFS) data were extracted using the XAFS program (Winterer, 1997). X-ray Absorption Near Edge Structure (XANES) and k^3-weighted EXAFS spectra were analyzed using a linear combination fit (LCF) procedure thanks to a custom-built software based on the Levenberg-Marquardt minimization algorithm. For this LCF analysis, we used experimental spectra from a large set of Fe-mineral model compounds (Cosmidis et al., 2014; Maillot et al., 2013, 2011; Noël et al., 2014), among which the following were retained in the fits: 2-line ferrihydrite (Maillot et al., 2011), Al-ferrihydrite (Al/Fe = 0.44) and Si-ferrihydrite (Si/Fe ~ 0.8) (Adra et al., 2013), schwertmannite (Adra et al., 2013; Maillot et al., 2013). These reference compounds are referred to as Fh, Fh-Al, Fh-Si and Schw in the following text, respectively. LCF fit quality was estimated by a reduced chi-square $\chi^2_R = \frac{N_{ind}}{(N_{ind}-Np)N_{points}} \frac{1}{\varepsilon^2} \sum (k^3\chi_{exp}(k) - k^3\chi_{calc}(k))^2$, where $N_{\mathrm{ind}} = (2\Delta k \Delta R/\pi)$ is the number of independent parameters, N_p is the number of fitting components for which a fraction p is refined, N_{points} the number of data points and ε is the measurement uncertainty (Ravel and Newville, 2005). The ε value was estimated as the root mean square of the Fourier back-transform of the data in the 15-25 Å R-range. Uncertainty on each refined parameter p was estimated as $3 \times \sqrt{VAR(p)\,\chi^2_R}$, where *VAR(p)* is the variance of parameter p returned by the Levenberg–Marquardt routine for the lowest χ^2_R.

ACCEPTED MANUSCRIPT

2.3. Transmission Electron Microscopy

For Transmission Electron Microscopy (TEM) analyses, lake water samples were centrifuged in an anoxic glovebox ($p(O_2)$<50 ppm) and rinsed twice with deoxygenated mQ water (with pH adjusted to the lake water pH). A drop of sample was deposited on 200-mesh Formvar carbon-coated or Lacey carbon-coated copper TEM grids. TEM grids were kept under anoxic conditions until transfer to the TEM chamber and analyses.

TEM, High Resolution TEM (HRTEM), Scanning Transmission Electron Microscopy (STEM) and Energy-Dispersive X-ray Spectroscopy (EDXS) were performed with a JEOL 2100F Microscope, operating at 200 kV. STEM analyses were conducted in high angle annular dark field (HAADF) mode. EDXS maps were acquired in STEM HAADF mode, with a focused electron beam (1 – 1.5 nm). Selected area diffraction (SAED) patterns were obtained on areas of interest.

2.4. Scanning Transmission X-ray Microscopy

Samples were analysed using Scanning Transmission X-ray Microscopy (STXM) at the Fe $L_{2,3}$-edges and C K-edge (Cosmidis and Benzerara, 2014). Samples were prepared as described earlier (Miot et al., 2009a; Miot et al., 2014). Briefly, samples were centrifuged and rinsed in the glovebox as for TEM preparation. A drop of sample was then deposited in between two Si_3N_4 windows (Norcada, Canada). As prepared Si_3N_4 sandwiches were then kept in anoxic aluminum pockets for transfer to the synchrotron. The microscope chamber was flushed with N_2 before and during transfer of the sample holders. Analyses were performed either under vacuum or under He atmosphere to prevent sample oxidation.

ACCEPTED MANUSCRIPT

Part of the STXM analyses at the Fe $L_{2,3}$-edges were performed at the Swiss Light Source (SLS, Villigen, Switzerland) on the PolLuX beamline. Part of analyses at the Fe $L_{2,3}$-edges and all analyses at the C K-edge were performed at the Canadian Light Source (CLS, Saskatoon, Canada). Additional information on PolLux and SM beamlines can be found in (Bernard et al., 2007) and in (Kaznatcheev et al., 2007), respectively. Energy scales for this study were calibrated using the well-resolved 3p Rydberg peak of gaseous CO_2 for the C K-edge and the major peak of hematite at 708.5 eV for the Fe L_3-edge. Data were acquired at the C K-edge and Fe $L_{2,3}$-edges as described in (Miot et al., 2009a). Data (stacks and Near-Edge X-ray Absorption Fine Structure (XANES) spectra) were processed using the aXis2000 software package (Hitchcock, 2001) as described in (Miot et al., 2009a). More recent analytical details on STXM data processing for the determination of Fe redox state can be found in (Bourdelle et al., 2013).

3. Results

3.1. Water column chemistry and XAS analyses of bulk Fe mineralogy with depth

Water of lake 77 had the typical characteristics of a lignite mine lake with low pH (Fig. 1). In addition, this lake has been shown to display high concentrations of dissolved Fe(II) and sulfate (Reiche et al., 2011) (Fig. A.1). CB water of November 2013 was homogeneous over depth after autumn circulation (Fig. 1A) with a pH of 2.8 throughout the oxic water body. The oxygen content declined only slightly from 250 $\mu mol.L^{-1}$ to 215 $\mu mol.\ L^{-1}$ above the sediment. In contrast, lake stratification was still present in NB as indicated by the sharp decline in O_2 concentration to less than 6 $\mu mol.L^{-1}$ from 5.2 to 5.7-m depth. The pH of the upper water body showed characteristics similar to CB water

ACCEPTED MANUSCRIPT

with a pH of 2.8, whereas the separated anoxic hypolimnion had a pH of 5.4 and slightly more elevated temperature and conductivity (Fig. 1B).

In September 2014, the acidic CB water body was stratified (Fig. 1C), with an oxycline extending from 4.8 down to 6-m depth, where dissolved oxygen reached less than 6 $\mu mol.L^{-1}$). The oxycline in NB had moved up to 4.2 to 4.7-m depth (Fig. 1D) associated with sharp gradients of pH reaching a maximum value of 5.5 in the anoxic hypolimnion. Dissolved Fe(II) and sulfate concentrations measured in NB in September 2014 increased up to 10.7 $mmol.L^{-1}$ and 28.3 $mmol.L^{-1}$ respectively in the hypolimnion (Fig. A.1), in accordance with previously published more extensive geochemical analyses of NB (and CB) water columns (Reiche et al., 2011).

The mineralogy of Fe bearing phases was investigated as a function of depth at these two basins in September 2014. X-ray Absorption Spectroscopy (XAS) at the Fe K-edge provided insight into the nature of Fe minerals, including amorphous or poorly crystalline phases (Fig. 2). The spectra of the samples collected in the mixolimnion of NB (i.e., above the oxycline, NB-4.9m-2014) and in the hypolimnion of CB (i.e., below the oxycline, CB-6.0m-2014) were rather similar based on Linear Combination Fits (LCF) of their EXAFS and XANES spectra indicating that 100% of the iron was present as schwertmannnite (Fig. 2). In contrast, a major ferrihydrite contribution was observed in the monimolimnion of NB (i.e. below the oxycline, NB-6.0m-2014). The best fit (χ^2_R = 0.21) of NB-6.0m-2014 EXAFS spectrum was obtained with a combination of 40 ± 6% schwertmannite and 61 ± 8% aluminous ferrihydrite (Fig. 2). Other fit solutions including a combination of schwertmannite (Schw) with 2-line ferrihydrite (Fh) or with Si-bearing ferrihydrite (Fh-Si) were acceptable but gave slightly poorer fits (Fig. A.2). However, Fh and Fh-Si local structures were likely present in the CB-6.0m-2014 iron precipitate, though their proportions cannot be determined with enough accuracy.

ACCEPTED MANUSCRIPT

Indeed, including Fh or Fh-Si as a third fitting component in addition to Schw and Fh-Al gave slightly better match to the data than the two-component fit solution but did not significantly improve the reduced chi2 value (Fig. A.2). Fit solutions using goethite instead of schwertmannite were systematically of poorer quality, knowing that the EXAFS spectra of these two phases can be clearly distinguished over the large *k*-range investigated here (Fig. A.3). Moreover, for the three studied samples, attempts to include goethite (Gt) as a fitting component were unsuccessful when schwertmannite was also included as a component. In this case, the fitted goethite proportion systematically vanished. These results indicate that goethite was absent from the samples studied.

3.2. STXM analyses of Fe and C speciation down to the sub-micrometer scale

To get further insight into the speciation of Fe down to the sub-micrometer scale, we performed STXM analyses at the Fe $L_{2,3}$-edges. As the core of schwertmannite particles was very thick, saturation effects prevented us to accurately determine its Fe redox state. Nevertheless, areas at the periphery of the schwertmannite particles or isolated thinner particles could be analyzed accurately. We observed notable differences from one sample to another. Based on their XANES Fe $L_{2,3}$-edges spectra, all areas analyzed in samples from NB (November 2013 and September 2014) exhibited a mostly Fe(III) redox state (Fig. 3). But a few particles from the monimolimnion of NB exhibited a mixed Fe valence state, with an estimated FeII/(FeII+FeIII) ratio up to ½ in some areas (Fig. 3). Although this result was only obtained on a few particles this suggests that the redox state of Fe may locally shift to reduced Fe valence below the oxycline in NB. In contrast, we were not able to find particles with FeII/(FeII+FeIII) ratios higher

ACCEPTED MANUSCRIPT

than 20% in the samples collected below the oxycline of CB (in November 2013 and September 2014) (Fig. 4).

Using TEM, some bacteria were observed in close proximity with the Fe minerals (Fig. 5A-B). In order to localize them more accurately and explore C speciation, we conducted STXM analyses at the C K-edge on selected samples from NB and CB in September 2014. Fe minerals were associated with high amounts of organic matter. In particular, multiple bacteria could be localized in association with the Fe-rich aggregates (Fig. 6). Their C K-edge XANES spectra exhibited a maximum of absorbance at 288.2 eV corresponding to the 1s—π * electronic transitions of amide bonds, usually attributed to maximum absorption of the peptidic bonds in proteins. Maxima at 285 eV and 287 eV could be attributed to alkene (C=C) and aliphatic (C-C) or carbonyl (C=O) functionnal groups respectively. These XANES spectra were thus fully consistent with the signature of bacteria (Benzerara et al., 2004). In addition, the large peak in the 288-290 eV region may include contributions of 1s—π * electronic transitions of carboxylic functions at 288.6 eV (Miot et al., 2009b) as well as 1s—π * electronic transitions of alcohol groups at 289.2 eV (Bernard et al., 2010) consistent with the maximum absorption of reference polysaccharidic compounds. Extracellular polymeric substances (EPS) were thus present as well, in accordance with the large amount of organic matter exhibiting no specific bacterial morphology and associated with Fe precipitates (Fig. 6).

3.3. Properties of Fe minerals down to the atomic scale

Schwertmannite particles composing iron snow from CB and NB consisted in aggregates of needles. High resolution TEM analyses of needles from CB yield either

ACCEPTED MANUSCRIPT

poorly crystalline (at 5.6-m depth, Fig. 7A-B) or nanocrystalline (at 6.0-m depth, Fig. 7C-D) electron diffraction patterns. FFT pattern in Fig. 7D yield *d*-spacings at 2.5 and 1.95 Å consistent with the (212) and (113) planes of schwertmannite. Noteworthy, fringes in the HRTEM images could only be observed in areas of a few nm (2-5 nm), showing that the needles were composed of multiple nanocrystals adjacent to each other. In addition, needles exhibited an amorphous layer on their periphery. These samples had homogeneous chemical compositions, with S/Fe atomic ratios consistent with schwertmannite (e.g. S/Fe = 0.12 as shown by EDXS in sample NB4.9m-2014, Fig. 8A-D). Consistently with XAS and STXM analyses, the mineralogy of samples collected in CB and in the epilimnion of NB was thus very homogeneous and restricted to schwertmannite.

In contrast, particles collected from the monimolimnion of NB (6.0-m depth) exhibited two types of morphologies (Fig. 5C-E):

(1) "Hedgehog" thick particles, consisting in aggregates of needles (typical schwertmannite texture, (Cornell and Schwertmann, 2003)). Each needle measured a few nm in thickness and a few hundreds of nm in length. These aggregates exhibited either amorphous or polycrystalline electron diffraction patterns (Fig. 5D-E). Polycrystalline patterns were consistent with schwertmannite. For example needles from hedgehog particles presented in Fig. 9A-B had *d*-spacings of around 3.3 Å, consistent with the (310) planes of schwertmannite. FFT patterns were also consistent with a schwertmannite structure (Fig. 9C).

(2) Round particles of around 50 nm in diameter exhibited systematically an amorphous electron diffraction pattern. As shown by STEM imaging and EDXS mapping, these round particles were associated with electron dense nanoparticles of around 4-10 nm in diameter at their surfaces (Fig. 8E-F). EDXS analyses indicated that these electron

ACCEPTED MANUSCRIPT

dense nanoparticles have a higher S/Fe ratio (S/Fe=0.2) than the electron lighter particles measuring 50 nm in diameter (S/Fe = 0.08) (Fig. 8G-H). Although the morphology of these electron dense nanoparticles was not consistent with schwertmannite needles, their S/Fe atomic ratios were consistent with the chemical composition of schwertmannite. In addition, S-rich and S-poor particles exhibited similar Si/Fe (Si/Fe = 0.2) and Al/Fe ratios (Al/Fe = 0.1 to 0.15). Finally, HRTEM indicated that the electron dense nanoparticles exhibited a schwertmannite structure. For instance, the particles from Fig. 9D-F had *d*-spacings consistent with the (310) and (212) planes of schwertmannite at 3.39 and 2.55 Å respectively. In contrast, the electron lighter S-poor particles were systematically amorphous (Fig. 9D-E). In summary, besides schwertmannite needles, the NB-6.0m-2014 sample contained electron dense S-rich (S/Fe consistent with schwertmannite composition) nanoparticles (4-10 nm in diameter) exhibiting a schwertmannite crystal structure associated with amorphous S-poor larger (50 nm in diameter) particles.

4. Discussion

4.1. Schwertmannite, a major polycrystalline mineral phase in lake 77

Chemical conditions in Lausatian lake 77 (low pH (Fig. 1) and high concentrations in dissolved Fe(II) and sulfate (Reiche et al., 2011) (Fig. A.1)) are predicted to promote the formation of schwertmannite (Bigham et al., 1996). Given the acidic conditions of the lake, this precipitation is mainly driven by microbial Fe(II) oxidation (Lu et al., 2013; Reiche et al., 2011) and EPS observed in association with schwertmannite particles might play a role in their nucleation (Hallberg, 2010; Hedrich

ACCEPTED MANUSCRIPT

et al., 2011) (Fig. 6). Present XAS and TEM results indicated that schwertmannite was the predominant Fe mineral in the water column of this lake. It was the only phase detected by XAS in the epilimnion of both CB and NB and this phase remained predominant in the hypolimnion of CB in September 2014 (100% schwertmannite, Fig. 2). These results are consistent with previous Raman analyses of iron snow from lake 77 (Ciobotă et al., 2013). However, schwertmannite represented only 40% of the Fe-bearing phases in the monimolimnion of NB in September 2014 (Fig. 2), with the other 60% being in the form of ferrihydrite. In contrast, ferrihydrite was identified at extremely low concentrations in samples from the same sampling site using Raman spectroscopy (Ciobotă et al., 2013). This could be explained either by different chemical conditions in this deep part of the lake that is disconnected from the rest of the water column and/or by the difficulty to accurately distinguish ferrihydrite from schwertmannite using Raman spectroscopy (due to band overlap in the 700 cm^{-1} region), especially in cases where schwertmannite and ferrihydrite are intimately associated down to the few nanometer-scale, as exemplified by present STEM and HRTEM analyses (Fig. 8-9).

The structure and stability of schwertmannite have been deeply debated in the last years. Based on Pair Distribution Function (PDF) and X-ray diffraction (XRD) data, (Fernandez-Martinez et al., 2010) proposed that this mineral has an akaganeite-like structure, in which the frame of iron octahedra is deformed with respect to the ideal akaganeite structure. The similarity between the local structures of schwertmannite (Maillot et al., 2013) and akaganeite (Maillot et al., 2011) is supported by the similarity of their EXAFS spectra at the Fe K-edge (Adra et al., 2013; Waychunas et al., 1995). The short range (~3.5 Å) local structure around Fe^{3+} ion in akaganeite/schwertmannite is also similar to that in goethite (Maillot et al., 2013, 2011) with edge- and corner-sharing

ACCEPTED MANUSCRIPT

linkage between FeO_6 octahedra. However, the EXAFS spectra of small-particles goethite (MCD ~ 11-16 nm) differ from that of nanocrystalline akaganeite (MCD ~ 3-5 nm) / schwertmannite (MCD ~ 4-8 nm) (Maillot et al., 2013). This difference is caused by the decrease in crystallite size and also by the differences in medium-range structures (~ 4.5-6.0 Å) that can be evidenced through distinct long distance single and multiple scattering paths observed in EXAFS data collected over a large *k*-range at cryogenic temperature (Maillot et al., 2013, 2011). This difference between the EXAFS spectra of schwertmannite and goethite is illustrated in Figs. A.1 and A.2, which indicate that the best match for sample NB-6.0m-2014 is obtained with schwertmannite mixed with ferrihydrite. The difference between the local structures of akaganeite/schwertmannite and that of ferrihydrite is even more pronounced, when comparing their EXAFS spectra at the Fe K-edge (Maillot et al., 2011) since ferrihydrite has kegging local structure that consists of octahedrally and tetrahedrally coordinated Fe^{3+} ions (Maillot et al., 2011; Michel et al., 2007).

Different studies highlighted the heterogeneous structure and chemical composition of schwertmannite, which may account for its wide range of solubility products (from $10^{-5.8}$ to $10^{-39.5}$) (Bigham et al., 1996; Caraballo et al., 2013; Kawano and Tomita, 2001; Majzlan et al., 2004; Yu et al., 1999). On the basis of HRTEM observations, it has been proposed that schwertmannite would first form as an aggregate of ferrihydrite particles, that would thereafter grow needles consisting in packed nanocrystals of goethite (French et al., 2012; Hockridge et al., 2009). Local enrichment in sulfur was shown to be associated with the more structurally ordered nanodomains in schwertmannite particles (French et al., 2012). Such local sulfate enrichment may be explained by variations in the content of sulfate ions adsorbed at the surface of the mineral (Caraballo et al., 2009) or trapped within the channels formed by Fe octahedra

ACCEPTED MANUSCRIPT

(Fernandez-Martinez et al., 2010). Based on such strong variations in S/Fe ratios in schwertmannite (Caraballo et al., 2013) have recently suggested that this mineral may be interpreted as a pseudo-solid solution. In contrast, some authors suggest that schwertmannite would not be a distinct mineral phase, but a mixture of ferrihydrite and goethite, with various amounts of adsorbed sulfate (Hockridge et al., 2009).

In the present study, we observed schwertmannite needles of a few hundreds of nm in length and a few nm in width, falling within the size ranges previously reported for this mineral (Bigham and Nordstrom, 2000; French et al., 2012). Whereas STEM / EDXS analyses revealed homogeneous Fe and S distributions in these needle-like schwertmannite aggregates (Fig. 8A-D), HRTEM analyses revealed that they consisted in aggregates of nanodomains each one exhibiting the crystal structure of schwertmannite (Fig. 7). Noteworthy, XAS analyses indicated that no goethite was present in these samples (Fig. A.3). Consistently *d*-spacings measured on HRTEM images did not provide distances all consistent with goethite planes, thus indicating that local order was not attributable to goethite. Thus schwermannite particles from lake 77 appear to form as a specific phase, enriched in sulfate ions, growing by aggregation of nanodomains.

4.2. Transformation of schwertmannite to ferrihydrite in lake 77

In the monimolimnion of NB, schwertmannite transformed into ferrihydrite, as evidenced by XAS (Fig. 2) and HRTEM analyses (Fig. 9). This transformation may be accounted for by the higher pH value around 5.5 and partial neutralization of lake water below the oxycline (Fig. 1). Indeed, ferrihydrite and goethite are usual products of schwertmannite transformation at pH > 4.5-6.0 and it has been proposed that schwertmannite transformation to ferrihydrite / goethite could proceed either by

ACCEPTED MANUSCRIPT

dissolution–reprecipitation or by local atomic rearrangement (Bigham et al., 1996; Burgos et al., 2012; Murad and Rojik, 2003; Sánchez-España et al., 2011). On the basis of recent PDF and EXAFS data on the structure of ferrihydrite (Maillot et al., 2011; Michel et al., 2007) and schwertmannite (Fernandez-Martinez et al., 2010; Maillot et al., 2013), it can be inferred that the similarities between the local structures of schwertmannite/akaganeite and goethite, with a similar hexagonal *ABAB* stacking of oxygen anions, could permit solid-state transformation. In contrast, the significant differences in short and medium-range local structures between schwertmannite/akaganeite and ferrihydrite (this latter phase having a double-hexagonal *ABAC* anionic stacking) suggest that schwertmannite to ferrihydrite transformation proceeds via dissolution-reprecipitation.

In the present study, HRTEM, STEM and EDXS analyses of the Fe precipitates in the monimolimnion of NB showed the presence of electron dense S-rich nanoparticles exhibiting a structure of schwertmannite that are embedded within an amorphous matrix (Fig. 8E-H, Fig. 9D-F). These nanoparticles could be relics of schwertmannite and/or transient phases between schwertmannite needles and ferrihydrite, the amorphous matrix being assigned to Al- and Si-containing ferrihydrite. These observations are consistent with a dissolution of schwertmannite accompanied by a release of the sulfate ions previously incorporated within the octahedral iron tunnel structure of schwertmannite or sorbed to its surface (Bigham et al., 1996), followed by the reprecipitation of Al- and Si-bearing ferrihydrite.

Transformation of schwertmannite to goethite/ferrihydrite can be accelerated in the presence of dissolved Fe(II) and absence of O_2 at near-neutral pH (Burton et al., 2008, 2007), i.e. under conditions similar to those of the monimolimnion water in NB (up to 12 mmol.L^{-1} dissolved Fe(II), no O_2, up to pH 5.5, Figure A.1). Indeed, an inflow of

ACCEPTED MANUSCRIPT

less acidic, Fe(II)- and sulfate-rich groundwater (pH 3.8, 3.5 mmol.L^{-1} dissolved Fe(II), 10 mmol.L^{-1} sulfate) has been reported in NB (Reiche et al., 2011) that would contribute to schwertmannite destabilization. In addition, organic matter associated with schwertmannite aggregates (Fig. 6) could be an attractive ecological niche for heterotrophs, such as acidophilic Fe(III)-reducers (Bertel et al., 2012; Blodau and Gatzek, 2006; Burton et al., 2013; Coupland and Johnson, 2008; Küsel et al., 1999) releasing additionnal Fe(II) as follows:

$$C_6H_{12}O_6 + 3\ Fe_8O_8(OH)_6(SO_4) + 36\ H^+ \rightarrow 6\ HCO_3^- + 24\ Fe^{2+} + 3\ SO_4^{2-} + 30\ H_2O \quad (1)$$

where $C_6H_{12}O_6$ stands not only for glucose but also for a generic formula of organic matter.

In NB, Fe(II) released by such a reaction would promote schwertmannite transformation to ferrihydrite through catalytic hydrolysis (Burton et al., 2008, 2007).

Furthermore, we did not detect any iron sulfide, contrary to usual observations of mackinawite (FeS) or greigite (Fe_3S_4) resulting from Fe(II) reaction with H_2S produced upon microbial sulfate reduction (Bertel et al., 2012; Burton et al., 2013). Low sulfate concentrations and highly acidic conditions would have prevented extensive microbial sulfate reduction in the water column of lake 77 (Blodau and Gatzek, 2006; Burton et al., 2013) and instead promoted the transformation of schwertmannite to ferrihydrite with no or minor associated iron sulfide. This is consistent with the fact that Fe(II) could not be detected using bulk XAS analyses at the Fe K-edge (Fig. 2), indicating that Fe(II) would necessarily be present at low levels (< 10%) in the particulate matter (Seder-Colomina et al., 2015). Nevertheless, although STXM analyses confirmed the predominance of Fe(III), we observed a few areas exhibiting local mixed Fe valence, with Fe(II)/(Fe(II)+Fe(III)) ratios up to 0.5 in NB and 0.2 in CB (Fig. 3 and Fig. 4). We

ACCEPTED MANUSCRIPT

can hypothesize that these mixed valence Fe-bearing particles may contain minor amounts of Fe(II) phases associated with schwertmannite and/or ferrihydrite. For instance, available water chemistry data (Fig. A.1 and Reiche et al., 2011) indicate that NB monimolimnion is supersaturated with respect to siderite (SI~20). In contrast, potential formation of vivianite or Fe(II,III) phosphates (Cosmidis et al., 2014) would be necessarily limited to trace amounts, since the particulate matter contains less than 200 ppm P (Lu et al., 2013). In addition, Fe redox state in the core of the thickest iron snow aggregates could not be determined using STXM because of thickness / saturation issues. If Fe(III) reducers inhabited the core of the iron snow aggregates in lake 77, we would thus have missed most of ferrihydrite and potential Fe(II) phases. Elucidating the links between microbial diversity and local Fe redox state / mineralogy within iron snow aggregates (Elliott et al., 2014) remains a critical issue that would deserve future in-depth investigations.

In CB, no transformation of schwertmannite could be observed, most probably related to (i) the persistence of very acidic conditions (Fig. 1), (ii) the absence of Fe(II)-rich groundwater inflow at this location (Reiche et al., 2011) and (iii) the short residence time of iron snow within the lake water column limiting the extent of microbial Fe(III) reduction (Lu et al., 2013; Reiche et al., 2011) all favorable to the stability of schwertmannite.

4.3. Stability of schwertmannite and ferrihydrite in northern basin of lake 77

The stability of schwertmannite is controlled by structural, thermodynamic and kinetic parameters. Transformation to crystalline goethite is usually observed upon neutralization (Bigham et al., 1996; Burgos et al., 2012) sometimes leading to the

ACCEPTED MANUSCRIPT

production of traces of ferrihydrite in addition to goethite (Paikaray and Peiffer, 2012). Here, we did not observe the transformation of schwertmannite to goethite, but only to ferrihydrite in the monimolimnion of NB. Whereas goethite/ferrihydrite formation is thermodynamically favorable under conditions where schwertmannite precipitates, transformation of schwertmannite to goethite is kinetically controlled. These kinetics vary from hours to years depending on the studies and conditions (Acero et al., 2006; Burton et al., 2008, 2007; Knorr and Blodau, 2007; Regenspurg et al., 2004; Schwertmann and Carlson, 2005). The fast sedimentation rates of iron snow particles (only several hours for a single particle to settle through the whole water column) in lake 77 (Reiche et al., 2011) might be too short to allow the transformation of schwertmannite to goethite. However, we can not exclude that ferrihydrite conversion to goethite (Banfield, 2000; Burleson and Penn, 2006) might occur deeper in the NB water column, e.g. at the sediment/water interface or within the sediment. In addition, transformation to goethite within the water column may be hindered by schwertmannite and ferrihydrite stabilization. Silicate (Anderson and Benjamin, 1985; Cornell et al., 1987), organic matter (Cornell and Schwertmann, 1979; Kodama and Schnitzer, 1977; Schwertmann, 1966) and phosphate (Barron et al., 1997) can sorb at the surface of ferrihydrite. In addition, silicate and aluminum may sorb onto schwertmannite (Collins et al., 2010). Given the high specific surface areas of these two minerals, such adsorption processes can immobilize a significant amount of these elements. In addition, although Al^{3+} cations could theoritically substitute for Fe^{3+} within the structure of schwertmannite, such substitution has not been reported so far, whereas aluminous ferrihydrite has been reported from both synthetic and natural origin (Adra et al., 2013; Cismasu et al., 2012). This difference is likely related to the higher solubility of Al^{3+} minerals than Fe^{3+} mineral phases within the stability field of

ACCEPTED MANUSCRIPT

schwertmannite, i.e., at acidic pH. Accordingly, EXAFS analysis of ferrihydrite-schwertmannite mixtures from acid mine drainage indicated the coexistence of aluminous ferrihydrite with aluminum-free schwertmannite (Adra et al., 2013). In the same way, silicate may modify the local ferrihydrite structure, by inhibiting double corner Fe-Fe linkages at 3.45 Å (Adra et al., 2013; Doelsch et al., 2003; Pokrovski et al., 2003; Voegelin et al., 2010). In the present study Al and Si were associated with schwertmannite and ferrihydrite (Fig. 2 and 8). In addition, high amounts of organic matter were associated with Fe minerals (Fig. 6). Organic matter, aluminum and silicate sorbed to the surface of schwertmannite could limit its solubility and would thus prevent its transformation to goethite via dissolution-reprecipitation, in particular via Fe(II)-catalyzed hydrolysis (Collins et al., 2010; Jones et al., 2009). Moreover, it was shown that high levels of Al promote the stabilization of ferrihydrite and delay its transformation into more crystalline phases such as goethite (Adra et al., 2013; Taylor and Schwertmann, 1978). We thus suggest that schwertmannite transformation to ferrihydrite and further stabilization of ferrihydrite are mainly promoted by Al, Si and organic matter sorption at the surface of schwertmannite and by Si sorption and Al incorporation in neoformed ferrihydrite.

5. Conclusions

Schwertmannite was the main Fe mineral in the water column of lake 77. This mineral exhibited a polycrystalline structure, consisting in aggregates of adjacent nanodomains, each one exhibiting a schwertmannite crystallographic structure. Whereas this phase remained stable in the pH 3 hypolimnion of CB, it transformed to ferrihydrite in pH 5.5 monimolimnion of NB. The following scenario can be proposed to

ACCEPTED MANUSCRIPT

explain this mineralogical transformation: (1) Fe(II) is supplied from a groundwater inflow (Reiche et al., 2011) as well as through microbial Fe(III) reduction below the oxycline (Lu et al., 2013). Both processes promote the catalytic hydrolysis of schwertmannite and its subsequent destabilization. (2) In addition, microbial Fe(III) reduction may consume acidity and enhance pH increase up to values incompatible with schwertmannite stability (Bigham et al., 1996). (3) Schwertmannite would thus transform into ferrihydrite via dissolution-reprecipitation, releasing sulfate. (4) Ferrihydrite would be stabilized with respect to goethite by incorporation of aluminum, and sorption of silicate and high amounts of organic matter. (5) At the same time, sorption of aluminum, silicate and organic matter at the surface of schwertmannite would prevent its complete transformation. (6) Low pH conditions as well as high sedimentation rates and relatively low sulfate concentrations would limit microbial sulfate reduction. (7) As a consequence, only low amounts of Fe(II) would react with H_2S supplied by microbial sulfate reduction or with carbonate (e.g. released via microbial Fe(III) reduction) to precipitate in the form of reduced iron compounds such as iron sulfide or iron carbonate. Fe(II) bearing phases observed in the monimolimnion of NB would deserve more extensive analyses to clarify their nature and modes of formation.

ACCEPTED MANUSCRIPT

Acknowledgements

This work was supported by the ANR SRB project, grant ANR-14-CE33-0003-01 of the French Agence Nationale de la Recherche to JM. The JEOL JEM2100F at IMPMC was bought with support from Region Ile de France grant SESAME 2000 E 1435, INSU CNRS, INP CNRS and University Pierre et Marie Curie Paris 6. We thank Jean-Michel Guigner

ACCEPTED MANUSCRIPT

for his expert support of the TEM at IMPMC. Part of STXM analyses was performed at the SM beamline at CLS. The Canadian Light Source is supported by NSERC, CIHR, NRC and the University of Saskatchewan. Additionnal STXM analyses were carried out at beamline PolluX at the Swiss Light Source, Paul Scherrer Institut, Villigen, Switzerland. Benjamin Watts (SLS), Jian Wang (CLS) and Chithra Karunakaran (CLS) are gratefully acknowledged for their help in STXM data acquisition. The authors thank ELETTRA (Trieste, Italy) for having provided beamtime and Luca Olivi is greatly acknowledged for his support during XAS measurements.

ACCEPTED MANUSCRIPT

ACCEPTED MANUSCRIPT

References

Acero, P., Ayora, C., Torrentó, C., Nieto, J.-M., 2006. The behavior of trace elements during schwertmannite precipitation and subsequent transformation into goethite and jarosite. Geochim. Cosmochim. Acta 70, 4130–4139. doi:10.1016/j.gca.2006.06.1367

Adra, A., Morin, G., Ona-Nguema, G., Menguy, N., Maillot, F., Casiot, C., Bruneel, O., Lebrun, S., Juillot, F., Brest, J., 2013. Arsenic Scavenging by Aluminum-Substituted Ferrihydrites in a Circumneutral pH River Impacted by Acid Mine Drainage. Environ. Sci. Technol. 47, 12784–12792. doi:10.1021/es4020234

Anbar, A.D., Duan, Y., Lyons, T.W., Arnold, G.L., Kendall, B., Creaser, R.A., Kaufman, A.J., Gordon, G.W., Scott, C., Garvin, J., Buick, R., 2007. A Whiff of Oxygen Before the Great Oxidation Event? Science 317, 1903–1906. doi:10.1126/science.1140325

Anderson, P.R., Benjamin, M.M., 1985. Effects of silicon on the crystallization and adsorption properties of ferric oxides. Environ. Sci. Technol. Lett. 1048–1053.

Banfield, J.F., 2000. Aggregation-Based Crystal Growth and Microstructure Development in Natural Iron Oxyhydroxide Biomineralization Products. Science 289, 751–754. doi:10.1126/science.289.5480.751

Barron, V., Galvez, N., Hochella, Jr., M.F., Torrent, J., 1997. Epitaxial overgrowth of goethite on hematite synthesized in phosphate media: a scanning force and transmission electron microscopy study. Am. Mineral. 1091–1100.

Benzerara, K., Morin, G., Yoon, T.H., Miot, J., Tyliszczak, T., Casiot, C., Bruneel, O., Farges, F., Brown, G.E., 2008. Nanoscale study of As biomineralization in an acid mine drainage system. Geochim. Cosmochim. Acta 72, 3949–3963. doi:10.1016/j.gca.2008.05.046

Benzerara, K., Yoon, T.H., Tyliszczak, T., Constantz, B., Spormann, A.M., Brown, G.E., 2004. Scanning transmission X-ray microscopy study of microbial calcification. Geobiology 2, 249–259. doi:10.1111/j.1472-4677.2004.00039.x

Bernard, S., Benzerara, K., Beyssac, O., Menguy, N., Guyot, F., Brown, G.E., Goffé, B., 2007. Exceptionnal preservation of fossil plant spores in high-pressure metamorphic rocks. Earth Planet. Sci. Lett. 257–272.

Bernard, S., Beyssac, O., Benzerara, K., Findling, N., Tzvetkov, G., Brown, G.E., 2010. XANES, Raman and XRD study of anthracene-based cokes and saccharose-based chars submitted to high-temperature pyrolysis. Carbon 48, 2506–2516. doi:10.1016/j.carbon.2010.03.024

Bertel, D., Peck, J., Quick, T.J., Senko, J.M., 2012. Iron Transformations Induced by an Acid-Tolerant Desulfosporosinus Species. Appl. Environ. Microbiol. 78, 81–88. doi:10.1128/AEM.06337-11

Bigham, J.M., Carlson, L., Murad, E., 1994. Schwertmannite, a new iron oxyhydroxysulphate from Pyhäsalmi, Finland, and other localities. Mineral. Mag. 641–648.

Bigham, J.M., Nordstrom, D.K., 2000. Iron and aluminum hydroxysulfates from acid sulfate waters, in: Alpers, C.N., Jambor, J.L., Nordstrom, D.K. (Eds.), Sulfate Minerals - Crystallography, Geochemistry, and Environmental Significance. Washington, DC.

Bigham, J.M., Schwertmann, U., Traina, S.J., Winland, R.L., Wolf, M., 1996. Schwertmannite and the chemical modeling of iron in acid sulfate waters. Geochim. Cosmochim. Acta 2111–2121.

Bingjie, O., Xiancai, L., Huan, L., Juan, L., Tingting, Z., Xiangyu, Z., Jianjun, L., Rucheng, W., 2014. Reduction of jarosite by Shewanella oneidensis MR-1 and secondary mineralization. Geochim. Cosmochim. Acta 124, 54–71. doi:10.1016/j.gca.2013.09.020

Blodau, C., 2006. A review of acidity generation and consumption in acidic coal mine

ACCEPTED MANUSCRIPT

lakes and their watersheds. Sci. Total Environ. 369, 307–332. doi:10.1016/j.scitotenv.2006.05.004
Blodau, C., Gatzek, C., 2006. Chemical controls on iron reduction in schwertmannite-rich sediments. Chem. Geol. 235, 366–376. doi:10.1016/j.chemgeo.2006.08.003
Bonnefoy, V., Holmes, D.S., 2012. Genomic insights into microbial iron oxidation and iron uptake strategies in extremely acidic environments: Iron oxidation and iron homeostasis in acidophiles. Environ. Microbiol. 14, 1597–1611. doi:10.1111/j.1462-2920.2011.02626.x
Bourdelle, F., Benzerara, K., Beyssac, O., Cosmidis, J., Neuville, D.R., Brown, G.E., Paineau, E., 2013. Quantification of the ferric/ferrous iron ratio in silicates by scanning transmission X-ray microscopy at the Fe L2,3 edges. Contrib. Mineral. Petrol. 166, 423–434. doi:10.1007/s00410-013-0883-4
Burgos, W.D., Borch, T., Troyer, L.D., Luan, F., Larson, L.N., Brown, J.F., Lambson, J., Shimizu, M., 2012. Schwertmannite and Fe oxides formed by biological low-pH Fe(II) oxidation versus abiotic neutralization: Impact on trace metal sequestration. Geochim. Cosmochim. Acta 76, 29–44. doi:10.1016/j.gca.2011.10.015
Burleson, D.J., Penn, R.L., 2006. Two-Step Growth of Goethite from Ferrihydrite. Langmuir 22, 402–409. doi:10.1021/la051883g
Burton, E.D., Bush, R.T., Sullivan, L.A., Mitchell, D.R.G., 2008. Schwertmannite transformation to goethite via the Fe(II) pathway: Reaction rates and implications for iron–sulfide formation. Geochim. Cosmochim. Acta 72, 4551–4564. doi:10.1016/j.gca.2008.06.019
Burton, E.D., Bush, R.T., Sullivan, L.A., Mitchell, D.R.G., 2007. Reductive transformation of iron and sulfur in schwertmannite-rich accumulations associated with acidified coastal lowlands. Geochim. Cosmochim. Acta 71, 4456–4473. doi:10.1016/j.gca.2007.07.007
Burton, E.D., Johnston, S.G., Kraal, P., Bush, R.T., Claff, S., 2013. Sulfate Availability Drives Divergent Evolution of Arsenic Speciation during Microbially Mediated Reductive Transformation of Schwertmannite. Environ. Sci. Technol. 47, 2221–2229. doi:10.1021/es303867t
Busigny, V., Planavsky, N.J., Jézéquel, D., Crowe, S., Louvat, P., Moureau, J., Viollier, E., Lyons, T.W., 2014. Iron isotopes in an Archean ocean analogue. Geochim. Cosmochim. Acta 133, 443–462. doi:10.1016/j.gca.2014.03.004
Canfield, D.E., Poulton, S.W., Knoll, A.H., Narbonne, G.M., Ross, G., Goldberg, T., Strauss, H., 2008. Ferruginous Conditions Dominated Later Neoproterozoic Deep-Water Chemistry. Science 321, 949–952. doi:10.1126/science.1154499
Caraballo, M.A., Rimstidt, J.D., Macías, F., Nieto, J.M., Hochella, M.F., 2013. Metastability, nanocrystallinity and pseudo-solid solution effects on the understanding of schwertmannite solubility. Chem. Geol. 360-361, 22–31. doi:10.1016/j.chemgeo.2013.09.023
Caraballo, M.A., Rotting, T.S., Nieto, J.M., Ayora, C., 2009. Sequential extraction and DXRD applicability to poorly crystalline Fe- and Al-phase characterization from an acid mine water passive remediation system. Am. Mineral. 1029–1038.
Carlson, L., Bigham, J.M., Schwertmann, U., Kyek, A., Wagner, F., 2002. Scavenging of As from Acid Mine Drainage by Schwertmannite and Ferrihydrite: A Comparison with Synthetic Analogues. Environ. Sci. Technol. 36, 1712–1719. doi:10.1021/es0110271
Ciobotă, V., Lu, S., Tarcea, N., Rösch, P., Küsel, K., Popp, J., 2013. Quantification of the inorganic phase of the pelagic aggregates from an iron contaminated lake by means of Raman spectroscopy. Vib. Spectrosc. 68, 212–219. doi:10.1016/j.vibspec.2013.08.005
Cismasu, A.C., Michel, F.M., Stebbins, J.F., Levard, C., Brown, G.E., 2012. Properties of

ACCEPTED MANUSCRIPT

impurity-bearing ferrihydrite I. Effects of Al content and precipitation rate on the structure of 2-line ferrihydrite. Geochim. Cosmochim. Acta 92, 275–291. doi:10.1016/j.gca.2012.06.010
Clarke, W.A., Konhauser, K.O., Thomas, J.C., Bottrell, S.H., 1997. Ferric hydroxide and ferric hydroxysulfate precipitaton by bacteria in an acid mine drainage lagoon. FEMS Microbiol. Rev. 351–361.
Collins, R.N., Jones, A.M., Waite, T.D., 2010. Schwertmannite stability in acidified coastal environments. Geochim. Cosmochim. Acta 74, 482–496. doi:10.1016/j.gca.2009.10.014
Cornell, R.M., Giovanoli, R., Schindler, P.W., 1987. Effect of silicate species on the transformation of ferrihydrite into goethite and hematite in alkaline media. Clays Clay Miner. 21–28.
Cornell, R.M., Schwertmann, U., 2003. The iron oxides: structure, properties, reactions, occurrences, and uses, 2nd, completely rev. and extended ed. ed. Wiley-VCH, Weinheim.
Cornell, R.M., Schwertmann, U., 1979. Influence of organic anions on the crystallization of ferrihydrite. Clays Clay Miner. 402–410.
Cosmidis, J., Benzerara, K., 2014. Soft X-ray scanning transmission spectromicroscopy, in: DiMasi, E., Gower, L.B. (Eds.), Biomineralization Sourcebook: Characterization of Biominerals and Biomimetic Materials. London, UK.
Cosmidis, J., Benzerara, K., Morin, G., Busigny, V., Lebeau, O., Jézéquel, D., Noël, V., Dublet, G., Othmane, G., 2014. Biomineralization of iron-phosphates in the water column of Lake Pavin (Massif Central, France). Geochim. Cosmochim. Acta 126, 78–96. doi:10.1016/j.gca.2013.10.037
Coupland, K., Johnson, D.B., 2008. Evidence that the potential for dissimilatory ferric iron reduction is widespread among acidophilic heterotrophic bacteria. FEMS Microbiol. Lett. 279, 30–35. doi:10.1111/j.1574-6968.2007.00998.x
Crowe, S.A., Døssing, L.N., Beukes, N.J., Bau, M., Kruger, S.J., Frei, R., Canfield, D.E., 2013. Atmospheric oxygenation three billion years ago. Nature 501, 535–538. doi:10.1038/nature12426
Crowe, S.A., O'Neill, A.H., Katsev, S., Hehanussa, P., Haffner, G.D., Sundby, B., Mucci, A., Fowle, D.A., 2008. The biogeochemistry of tropical lakes: A case study from Lake Matano, Indonesia. Limnol. Oceanogr. 53, 319–331.
Doelsch, E., Masion, A., Rose, J., Stone, W.E.E., Bottero, J.Y., Bertsch, P.M., 2003. Chemistry and structure of colloids obtained by hydrolysis of Fe(III) in the presence of SiO4 ligands. Colloids Surf. Physicochem. Eng. Asp. 217, 121–128. doi:10.1016/S0927-7757(02)00566-6
Egal, M., Casiot, C., Morin, G., Parmentier, M., Bruneel, O., Lebrun, S., Elbaz-Poulichet, F., 2009. Kinetic control on the formation of tooeleite, schwertmannite and jarosite by Acidithiobacillus ferrooxidans strains in an As(III)-rich acid mine water. Chem. Geol. 265, 432–441. doi:10.1016/j.chemgeo.2009.05.008
Elliott, A.V.C., Plach, J.M., Droppo, I.G., Warren, L.A., 2014. Collaborative microbial Fe-redox cycling by pelagic floc bacteria across wide ranging oxygenated aquatic systems. Chem. Geol. 366, 90–102. doi:10.1016/j.chemgeo.2013.11.017
Fernandez-Martinez, A., Timon, V., Roman-Ross, G., Cuello, G.J., Daniels, J.E., Ayora, C., 2010. The structure of schwertmannite, a nanocrystalline iron oxyhydroxysulfate. Am. Mineral. 95, 1312–1322. doi:10.2138/am.2010.3446
Fernández-Remolar, D.C., Morris, R.V., Gruener, J.E., Amils, R., Knoll, A.H., 2005. The Río Tinto Basin, Spain: Mineralogy, sedimentary geobiology, and implications for interpretation of outcrop rocks at Meridiani Planum, Mars. Earth Planet. Sci. Lett. 240, 149–167. doi:10.1016/j.epsl.2005.09.043

ACCEPTED MANUSCRIPT

Fleckenstein, J.H., Neumann, C., Volze, N., Beer, J., 2009. Raumzeitmuster des See-Grundwasser-Austausches in einem sauren Tagebaurestsee. Grundwasser 14, 207–217. doi:10.1007/s00767-009-0113-1
French, R.A., Caraballo, M.A., Kim, B., Rimstidt, J.D., Murayama, M., Hochella, M.F., 2012. The enigmatic iron oxyhydroxysulfate nanomineral schwertmannite: Morphology, structure, and composition. Am. Mineral. 97, 1469–1482. doi:10.2138/am.2012.4032
Gagliano, W.., Brill, M.., Bigham, J.., Jones, F.., Traina, S.., 2004. Chemistry and mineralogy of ochreous sediments in a constructed mine drainage wetland. Geochim. Cosmochim. Acta 68, 2119–2128. doi:10.1016/j.gca.2003.10.038
Hallberg, K.B., 2010. New perspectives in acid mine drainage microbiology. Hydrometallurgy 448–453.
Hedrich, S., Lünsdorf, H., Kleeberg, R., Heide, G., Seifert, J., Schlömann, M., 2011. Schwertmannite Formation Adjacent to Bacterial Cells in a Mine Water Treatment Plant and in Pure Cultures of *Ferrovum myxofaciens*. Environ. Sci. Technol. 45, 7685–7692. doi:10.1021/es201564g
Hitchcock, A.P., 2001. Soft X-ray spectromicroscopy of polymers and biopolymer interfaces. J. Synchrotron Radiat. 66–71.
Hockridge, J.G., Jones, F., Loan, M., Richmond, W.R., 2009. An electron microscopy study of the crystal growth of schwertmannite needles through oriented aggregation of goethite nanocrystals. J. Cryst. Growth 311, 3876–3882. doi:10.1016/j.jcrysgro.2009.06.023
Inskeep, W.P., Macur, R.E., Harrison, G., Bostick, B.C., Fendorf, S., 2004. Biomineralization of As(V)-hydrous ferric oxyhydroxide in microbial mats of an acid-sulfate-chloride geothermal spring, Yellowstone National Park. Geochim. Cosmochim. Acta 68, 3141–3155. doi:10.1016/j.gca.2003.09.020
Johnson, D.B., Kanao, T., Hedrich, S., 2012. Redox Transformations of Iron at Extremely Low pH: Fundamental and Applied Aspects. Front. Microbiol. 3. doi:10.3389/fmicb.2012.00096
Jones, A.M., Collins, R.N., Rose, J., Waite, T.D., 2009. The effect of silica and natural organic matter on the Fe(II)-catalysed transformation and reactivity of Fe(III) minerals. Geochim. Cosmochim. Acta 73, 4409–4422. doi:10.1016/j.gca.2009.04.025
Kawano, M., Tomita, K., 2001. Geochemical modeling of bacterially induced mineralization of schwertmannite and jarosite in sulfuric acid spring water. Am. Mineral. 1156–1165.
Kaznatcheev, K.V., Karunakaran, C., Lanke, U.D., Urquhart, S.G., Obst, M., Hitchcock, A.P., 2007. Soft X-ray spectromicroscopy beamline at the CLS: Commissioning results. Nucl. Instrum. Methods Phys. Res. Sect. Accel. Spectrometers Detect. Assoc. Equip. 582, 96–99. doi:10.1016/j.nima.2007.08.083
Knorr, K.-H., Blodau, C., 2007. Controls on schwertmannite transformation rates and products. Appl. Geochem. 22, 2006–2015. doi:10.1016/j.apgeochem.2007.04.017
Kodama, H., Schnitzer, M., 1977. Effect of fulvic acid on the crystallization of Fe(III) oxides. Geoderma 279–291.
Konhauser, K.O., Lalonde, S.V., Planavsky, N.J., Pecoits, E., Lyons, T.W., Mojzsis, S.J., Rouxel, O.J., Barley, M.E., Rosìere, C., Fralick, P.W., Kump, L.R., Bekker, A., 2011. Aerobic bacterial pyrite oxidation and acid rock drainage during the Great Oxidation Event. Nature 478, 369–373. doi:10.1038/nature10511
Küsel, K., 2003. Microbial cycling of iron and sulfur in acidic coal mining lake sediments. Water Air Soil Pollut. Focus 67–90.
Küsel, K., 2003. Microbial cycling of iron and sulfur in acidic coal mining lake sediments.

ACCEPTED MANUSCRIPT

Water. Air. Soil Pollut. 67–90.
Küsel, K., Dorsch, T., Acker, G., Stackebrandt, E., 1999. Microbial reduction of Fe(III) in acidic sediments: Isolation of Acidiphilum cryptum JF-5 capable of coupling the oxidation of glucose to the reduction of Fe(III). Appl. Environ. Microbiol. 3633–3640.
Lehours, A.-C., Bardot, C., Thenot, A., Debroas, D., Fonty, G., 2005. Anaerobic Microbial Communities in Lake Pavin, a Unique Meromictic Lake in France. Appl. Environ. Microbiol. 71, 7389–7400. doi:10.1128/AEM.71.11.7389-7400.2005
Lehours, A.-C., Batisson, I., Guedon, A., Mailhot, G., Fonty, G., 2009. Diversity of Culturable Bacteria, from the Anaerobic Zone of the Meromictic Lake Pavin, Able to Perform Dissimilatory-Iron Reduction in Different in Vitro Conditions. Geomicrobiol. J. 26, 212–223. doi:10.1080/01490450902744012
Lehours, A.-C., Evans, P., Bardot, C., Joblin, K., Gerard, F., 2007. Phylogenetic Diversity of Archaea and Bacteria in the Anoxic Zone of a Meromictic Lake (Lake Pavin, France). Appl. Environ. Microbiol. 73, 2016–2019. doi:10.1128/AEM.01490-06
Liao, Y., Zhou, L., Liang, J., Xiong, H., 2009. Biosynthesis of schwertmannite by Acidithiobacillus ferrooxidans cell suspensions under different pH condition. Mater. Sci. Eng. C 29, 211–215. doi:10.1016/j.msec.2008.06.011
Llirós, M., García–Armisen, T., Darchambeau, F., Morana, C., Triadó–Margarit, X., Inceoğlu, Ö., Borrego, C.M., Bouillon, S., Servais, P., Borges, A.V., Descy, J., Canfield, D.E., Crowe, S.A., 2015. Pelagic photoferrotrophy and iron cycling in a modern ferruginous basin. Sci. Rep. 5, 13803. doi:10.1038/srep13803
Lu, S., Chourey, K., Reiche, M., Nietzsche, S., Shah, M.B., Neu, T.R., Hettich, R.L., Küsel, K., 2013a. Insights into the Structure and Metabolic Function of Microbes That Shape Pelagic Iron-Rich Aggregates ("Iron Snow"). Appl. Environ. Microbiol. 79, 4272–4281. doi:10.1128/AEM.00467-13
Lu, S., Gischkat, S., Reiche, M., Akob, D.M., Hallberg, K.B., Küsel, K., 2010. Ecophysiology of Fe-Cycling Bacteria in Acidic Sediments. Appl. Environ. Microbiol. 76, 8174–8183. doi:10.1128/AEM.01931-10
Lu, X., Wang, H., 2012. Microbial Oxidation of Sulfide Tailings and the Environmental Consequences. Elements 8, 119–124. doi:10.2113/gselements.8.2.119
Maillot, F., Morin, G., Juillot, F., Bruneel, O., Casiot, C., Ona-Nguema, G., Wang, Y., Lebrun, S., Aubry, E., Vlaic, G., Brown, G.E., 2013. Structure and reactivity of As(III)- and As(V)-rich schwertmannites and amorphous ferric arsenate sulfate from the Carnoulès acid mine drainage, France: Comparison with biotic and abiotic model compounds and implications for As remediation. Geochim. Cosmochim. Acta 104, 310–329. doi:10.1016/j.gca.2012.11.016
Maillot, F., Morin, G., Wang, Y., Bonnin, D., Ildefonse, P., 2011. New insight into the structure of nanocrystalline ferrihydrite: EXAFS evidence for tetrahedrally coordinated iron(III). Geochim. Cosmochim. Acta 2708–2720.
Majzlan, J., Navrotsky, A., Schwertmann, U., 2004. Thermodynamics of iron oxides: Part III. Enthalpies of formation and stability of ferrihydrite (~Fe(OH)3), schwertmannite (~FeO(OH)3/4(SO4)1/8), and ε-Fe2O3. Geochim. Cosmochim. Acta 68, 1049–1059. doi:10.1016/S0016-7037(03)00371-5
Michel, F.M., Ehm, L., Antao, S.M., Lee, P.L., Chupas, P.J., Liu, G., Strongin, D.R., Schoonen, M.A.A., Phillips, B.L., Parise, J.B., 2007. The structure of ferrihydrite, a nanocrystalline material. Science 1726–1729.
Miot, J., Benzerara, K., Morin, G., Kappler, A., Bernard, S., Obst, M., Férard, C., Skouri-Panet, F., Guigner, J.-M., Posth, N., Galvez, M., Brown, G.E., Guyot, F., 2009a. Iron biomineralization by anaerobic neutrophilic iron-oxidizing bacteria. Geochim.

ACCEPTED MANUSCRIPT

Cosmochim. Acta 73, 696–711. doi:10.1016/j.gca.2008.10.033
Miot, J., Benzerara, K., Obst, M., Kappler, A., Hegler, F., Schadler, S., Bouchez, C., Guyot, F., Morin, G., 2009b. Extracellular Iron Biomineralization by Photoautotrophic Iron-Oxidizing Bacteria. Appl. Environ. Microbiol. 75, 5586–5591. doi:10.1128/AEM.00490-09
Miot, J., Jézéquel, D., Benzerara, K., Cordier, L., Rivas-Lamelo, S., Skouri-Panet, F., Férard, C., Poinsot, M., Duprat, E., 2016. Mineralogical Diversity in Lake Pavin: Connections with Water Column Chemistry and Biomineralization Processes. Minerals 6, 24. doi:10.3390/min6020024
Miot, J., Li, J., Benzerara, K., Sougrati, M.T., Ona-Nguema, G., Bernard, S., Jumas, J.-C., Guyot, F., 2014. Formation of single domain magnetite by green rust oxidation promoted by microbial anaerobic nitrate-dependent iron oxidation. Geochim. Cosmochim. Acta 139, 327–343. doi:10.1016/j.gca.2014.04.047
Mori, J.F., Lu, S., Händel, M., Totsche, K.U., Neu, T.R., Iancu, V.V., Tarcea, N., Popp, J., Küsel, K., 2015. Schwertmannite formation at cell junctions by a new filament-forming Fe(II)-oxidizing isolate affiliated with the novel genus Acidithrix. Microbiol. Read. Engl. doi:10.1099/mic.0.000205
Morin, G., Calas, G., 2006. Arsenic in Soils, Mine Tailings, and Former Industrial Sites. Elements 2, 97–101. doi:10.2113/gselements.2.2.97
Morin, G., Juillot, F., Casiot, C., Bruneel, O., Personné, J.-C., Elbaz-Poulichet, F., Leblanc, M., Ildefonse, P., Calas, G., 2003. Bacterial Formation of Tooeleite and Mixed Arsenic(III) or Arsenic(V)−Iron(III) Gels in the Carnoulès Acid Mine Drainage, France. A XANES, XRD, and SEM Study. Environ. Sci. Technol. 37, 1705–1712. doi:10.1021/es025688p
Morin, G., Rousse, G., Elkaim, E., 2007. Crystal structure of tooeleite, Fe6(AsO3)4SO4(OH)4{middle dot}4H2O, a new iron arsenite oxyhydroxy-sulfate mineral relevant to acid mine drainage. Am. Mineral. 92, 193–197. doi:10.2138/am.2007.2361
Murad, E., Rojik, P., 2003. Iron-rich precipitates in a mine drainage environment: Influence of pH on mineralogy. Am. Mineral. 1915–1918.
Neumann, C., Beer, J., Blodau, C., Peiffer, S., Fleckenstein, J.H., 2013. Spatial patterns of groundwater-lake exchange - implications for acid neutralization processes in an acid mine lake: IMPACTS OF GROUNDWATER-LAKE EXCHANGE ON ACID NEUTRALIZATION PROCESSES. Hydrol. Process. n/a–n/a. doi:10.1002/hyp.9656
Noël, V., Marchand, C., Juillot, F., Ona-Nguema, G., Viollier, E., Marakovic, G., Olivi, L., Delbes, L., Gelebart, F., Morin, G., 2014. EXAFS analysis of iron cycling in mangrove sediments downstream a lateritized ultramafic watershed (Vavouto Bay, New Caledonia). Geochim. Cosmochim. Acta 136, 211–228. doi:10.1016/j.gca.2014.03.019
Nordstrom, D.K., 2011. Hydrogeochemical processes governing the origin, transport and fate of major and trace elements from mine wastes and mineralized rock to surface waters. Appl. Geochem. 26, 1777–1791. doi:10.1016/j.apgeochem.2011.06.002
Nordstrom, D.K., Southam, G., 1997. Geomicrobiology of sulfide mineral oxidation, in: Geomicrobiology: Interactions between Microbes and Minerals, Reviews in Mineralogy. pp. 361–390.
Ohnuki, T., Sakamoto, F., Kozai, N., Ozaki, T., Yoshida, T., Narumi, I., Wakai, E., Sakai, T., Francis, A., 2004. Mechanisms of arsenic immobilization in a biomat from mine discharge water. Chem. Geol. 212, 279–290. doi:10.1016/j.chemgeo.2004.08.018
Paikaray, S., Peiffer, S., 2012. Abiotic schwertmannite transformation kinetics and the role of sorbed As(III). Appl. Geochem. 27, 590–597. doi:10.1016/j.apgeochem.2011.12.013

ACCEPTED MANUSCRIPT

Pokrovski, G.S., Schott, J., Farges, F., Hazemann, J.-L., 2003. Iron (III)-silica interactions in aqueous solution: insights from X-ray absorption fine structure spectroscopy. Geochim. Cosmochim. Acta 67, 3559–3573. doi:10.1016/S0016-7037(03)00160-1
Ravel, B., Newville, M., 2005. ATHENA, ARTEMIS, HEPHAESTUS: Data analysis for X-ray absorption spectroscopy using IFEFITT. J. Synchrotron Radiat. 537–541.
Regenspurg, S., Brand, A., Peiffer, S., 2004. Formation and stability of schwertmannite in acidic mining lakes. Geochim. Cosmochim. Acta 68, 1185–1197. doi:10.1016/j.gca.2003.07.015
Reiche, M., Lu, S., Ciobotă, V., Neu, T.R., Nietzsche, S., Rösch, P., Popp, J., Küsel, K., 2011. Pelagic boundary conditions affect the biological formation of iron-rich particles (iron snow) and their microbial communities. Limnol. Oceanogr. 56, 1386–1398. doi:10.4319/lo.2011.56.4.1386
Reinhard, C.T., Lalonde, S.V., Lyons, T.W., 2013. Oxidative sulfide dissolution on the early Earth. Chem. Geol. 362, 44–55. doi:10.1016/j.chemgeo.2013.10.006
Sánchez España, J., López Pamo, E., Santofimia, E., Aduvire, O., Reyes, J., Barettino, D., 2005. Acid mine drainage in the Iberian Pyrite Belt (Odiel river watershed, Huelva, SW Spain): Geochemistry, mineralogy and environmental implications. Appl. Geochem. 20, 1320–1356. doi:10.1016/j.apgeochem.2005.01.011
Sánchez-España, J., Yusta, I., Diez-Ercilla, M., 2011. Schwertmannite and hydrobasaluminite: A re-evaluation of their solubility and control on the iron and aluminium concentration in acidic pit lakes. Appl. Geochem. 26, 1752–1774. doi:10.1016/j.apgeochem.2011.06.020
Sánchez-España, J., Yusta, I., López, G.A., 2012. Schwertmannite to jarosite conversion in the water column of an acidic mine pit lake. Mineral. Mag. 76, 2659–2682. doi:10.1180/minmag.2012.076.7.03
Sandy Jones, F., Bigham, J.M., Gramp, J.P., Tuovinen, O.H., 2014. Synthesis and properties of ternary (K, NH4, H3O)-jarosites precipitated from Acidithiobacillus ferrooxidans cultures in simulated bioleaching solutions. Mater. Sci. Eng. C 44, 391–399. doi:10.1016/j.msec.2014.08.043
Schwertmann, U., 1966. Inhibitory effect of soil organic matter on the crystallization of amorphous ferrix hydroxide. Nature 645–646.
Schwertmann, U., Carlson, L., 2005. The pH-dependent transformation of schwertmannite to goethite at 25°C. Clay Miner. 63–66.
Seder-Colomina, M., Morin, G., Brest, J., Ona-Nguema, G., Gordien, N., Pernelle, J.-J., Banerjee, D., Mathon, O., Esposito, G., van Hullebusch, E.D., 2015. Uranium(VI) Scavenging by Amorphous Iron Phosphate Encrusting *Sphaerotilus natans* Filaments. Environ. Sci. Technol. 49, 14065–14075. doi:10.1021/acs.est.5b03148
Tabatabai, M.A., 1974. A Rapid Method for Determination of Sulfate in Water Samples. Environ. Lett. 7, 237–243. doi:10.1080/00139307409437403
Tamura, H., Goto, K., Yotsuyanagi, T., Nagayama, M., 1974. Spectrophotometric determination of iron(II) with 1,10-phenanthroline in the presence of large amounts of iron(III). Talanta 21, 314–318.
Taylor, R.M., Schwertmann, U., 1978. The influence of aluminum on iron oxides. Part I. The influence of Al on Fe oxide formation from the Fe(II) system. Clays Clay Miner. 373–383.
Viollier, E., Michard, G., Jézéquel, D., Pèpe, M., Sarazin, G., 1997. Geochemical study of a crater lake: lake Pavin, Puy de Dôme, France. Constraints afforded by the particulate matter distribution in the element cycling within the lake. Chem. Geol. 225–241.
Voegelin, A., Kaegi, R., Frommer, J., Vantelon, D., Hug, S.J., 2010. Effect of phosphate,

ACCEPTED MANUSCRIPT

silicate, and Ca on Fe(III)-precipitates formed in aerated Fe(II)- and As(III)-containing water studied by X-ray absorption spectroscopy. Geochim. Cosmochim. Acta 74, 164–186. doi:10.1016/j.gca.2009.09.020

Walter, X.A., Picazo, A., Miracle, M.R., Vicente, E., Camacho, A., Aragno, M., Zopfi, J., 2014. Phototrophic Fe(II)-oxidation in the chemocline of a ferruginous meromictic lake. Front. Microbiol. 5. doi:10.3389/fmicb.2014.00713

Waychunas, G.A., Xu, N., Fuller, C.C., Davis, J.A., Bigham, J.M., 1995. XAS study of AsO43– and SeO42– substituted schwertmannites. Phys. B Condens. Matter 208-209, 481–483. doi:10.1016/0921-4526(94)00730-J

Winterer, M., 1997. XAFS - a data analysis program for material science. J. Phys. Paris 243–244.

Xu, Y., Yang, M., Yao, T., Xiong, H., 2014. Isolation, identification and arsenic-resistance of Acidithiobacillus ferrooxidans HX3 producing schwertmannite. J. Environ. Sci. 26, 1463–1470. doi:10.1016/j.jes.2014.05.012

Yu, J.-Y., Heo, B., Choi, I.-K., Cho, J.-P., Chang, H.-W., 1999. Apparent solubilities of schwertmannite and ferrihydrite in natural stream waters polluted by mine drainages. Geochim. Cosmochim. Acta 3407–3416.

Zhu, J., Gan, M., Zhang, D., Hu, Y., Chai, L., 2013. The nature of schwertmannite and jarosite mediated by two strains of Acidothiobacillus ferrooxidans with different ferrous oxidation ability. Mater. Sci. Eng. C 2679–2685.

ACCEPTED MANUSCRIPT

ACCEPTED MANUSCRIPT

Figure captions

Figure 1. Geochemical profiles of CB (A and C) and NB (B and D) in November 2013 (A and B) and September 2014 (C and D): pH, dissolved oxygen ($mg.L^{-1}$), conductivity (mS/cm) and temperature (°C). The NB has an anoxic monimolimnion throughout the year. Arrows next to the dissolved oxygen plots indicate sampling depths.

Figure 2. Linear combination fits of Fe K-edge XANES (A) and EXAFS (B) spectra and corresponding Fast Fourier transforms (C) for samples from CB at 6.0-m depth (CB-6.0m-2014) and from NB at 4.9-m (NB-4.9m-2014) and 6.0-m depth (NB-6.0m-2014). Reference spectra and their relative proportions retrieved from LCF are displayed. Black line: data; Red line: fit.

Figure 3. STXM analyses at the Fe $L_{2,3}$-edges of samples collected from NB at 4.3 (NB-4.3m-2014), 4.5 (NB-4.5m-2013), 4.9 (NB-4.9m-2014) and 6.0 m depth (NB-6.0m-2013) respectively. (A): STXM map of the Fe component displayed in (C) on a particle from sample NB-4.5m-2013, (B): STXM map of the Fe component displayed in (C) on a particle from sample NB-6.0m-2013. (C): XANES spectra at the Fe $L_{2,3}$-edges of samples collected at different depths compared with reference compound spectra (goethite and vivianite).

Figure 4. STXM analyses at the Fe $L_{2,3}$-edges of samples collected from CB at 5.0 (CB-5.0m-2014) and 6.0 m depth (CB-6.0m-2013). (A, B): Fe maps of different particles from sample CB-6.0m-2013. (C): XANES spectra at the Fe $L_{2,3}$-edges of samples collected at 5.0

ACCEPTED MANUSCRIPT

(CB-5.0m-2014) and 6.0 m depth (CB-6.0m-2013) compared with reference compound spectra (goethite and vivianite $Fe^{II}_3(PO_4)_2 \bullet 8H_2O$).

Figure 5. TEM images of Fe-aggregates in sample NB-6.0m-2014. (A, B) : Bacteria associated with Fe rich particles. (C) Typical Fe-rich particles. (D, E) : Selected area diffraction patterns of particles circled in panel C.

Figure 6. Evidences of bacteria associated with Fe-rich aggregates in NB-4.9m-2014 (A, B) and CB-5.0m-2014 (C, D). Organic carbon maps (288.2 – 280 eV) (A, C) and corresponding Fe maps (710.3 – 690 eV) (B, D). (E): XANES C K-edge spectra of reference organic compounds (albumin, xanthan, alginate) and of the bright areas boxed in A and C.

Figure 7. HRTEM analyses of samples collected from CB at 5.6 m (CB-5.6m-2014) (A, B) and 6.0 m (CB-6.0m-2014) (C, D). Insets in (A) and (D) display FFT patterns corresponding to areas in white boxes. Inset in (C) is the SAED pattern obtained on needles from a « hedgehog » particle.

Figure 8. STEM-HAADF imaging and EDXS analyses of samples from NB at 4.9 m (NB-4.9m-2014) (A-D) and 6.0 m depth (NB-6.0m-2014) (E-H). (A, E, F): STEM images. (B, C, G) corresponding elemental maps (red: Fe, green: S). (D, H) EDXS spectra collected on needles in panel (A) (NB-4.9m-2014) and on the S-rich (electron dense spots) and S-poor (electron light matrix) areas in panel F (NB-6.0m-2014).

ACCEPTED MANUSCRIPT

Figure 9. HRTEM analyses of NB-6.0m-2014. (A) TEM image of Fe-rich aggregates. (B) is a magnified image of the area enclosed in the black box in (A), showing a crystalline particle within an amorphous matrix. (D): typical hedegehog morphology of a schwertmannite particle. (E) is a magnified view of the area within the black box in (D) showing the extremity of a single needle. (C) and (F) display the FFT patterns of the areas enclosed in white boxes in (B) and (E).

Appendices

Figure A.1 : Geochemical profile of NB in September 2014: pH, dissolved oxygen ($mg.L^{-1}$), dissolved Fe(II) ($mmol.L^{-1}$) and sulfate ($mmol.L^{-1}$) concentrations. Arrows next to the dissolved oxygen plot indicate sampling depths.

Figure A.2 : Linear combination fits of Fe K-edge EXAFS spectra (A) and corresponding Fast Fourier transforms (B) for samples from NB at 6.0-m depth (NB-6.0m-2014) using goethite in combination with various ferrihydrites as reference compounds. Reference spectra and their relative proportions retrieved from LCF are displayed. Black line: data; Red line: fit. The best two-component fit was obtained with Schw and Fh-Al. However, other fit solutions with Fh-Al or Fh-Si could not be excluded since they gave χ^2_R values that did not statistically differ from that of the best fit, with regard to a F-test at 5% confidence interval (i.e. an improvement of 60% of the χ^2_R would be expected in our case to reject the null hypothesis). The three-component fit only slightly improved the χ^2_R value (0.18), which also fell below the significance limit of the F-test, and the

ACCEPTED MANUSCRIPT

uncertainty on the fitted proportion of the two types of Fh was large. Thus, we did not retain this three-component fit solution. Other three-component fit solutions gave poorer results with respect to the F-test.

Figure A.3 : Linear combination fits of Fe K-edge EXAFS spectra (A) and corresponding Fast Fourier transforms (B) for samples from CB and NB at 6.0-m depth using either schwertmannite or goethite, alone and in combination with aluminous ferrihydrite, as fitting components. Black line: data; Red line: fit. The fit solutions with schwertmannite systematically better matched the data than the ones with goethite. Indeed the Gt spectrum clearly mismatches the CB-6m spectrum. For the NB-6m sample, χ^2_R is improved by 61% with the Schw fit solution and the better match to the data is especially obvious in the 3.5-5.5 Å *R*-range.

ACCEPTED MANUSCRIPT

ACCEPTED MANUSCRIPT

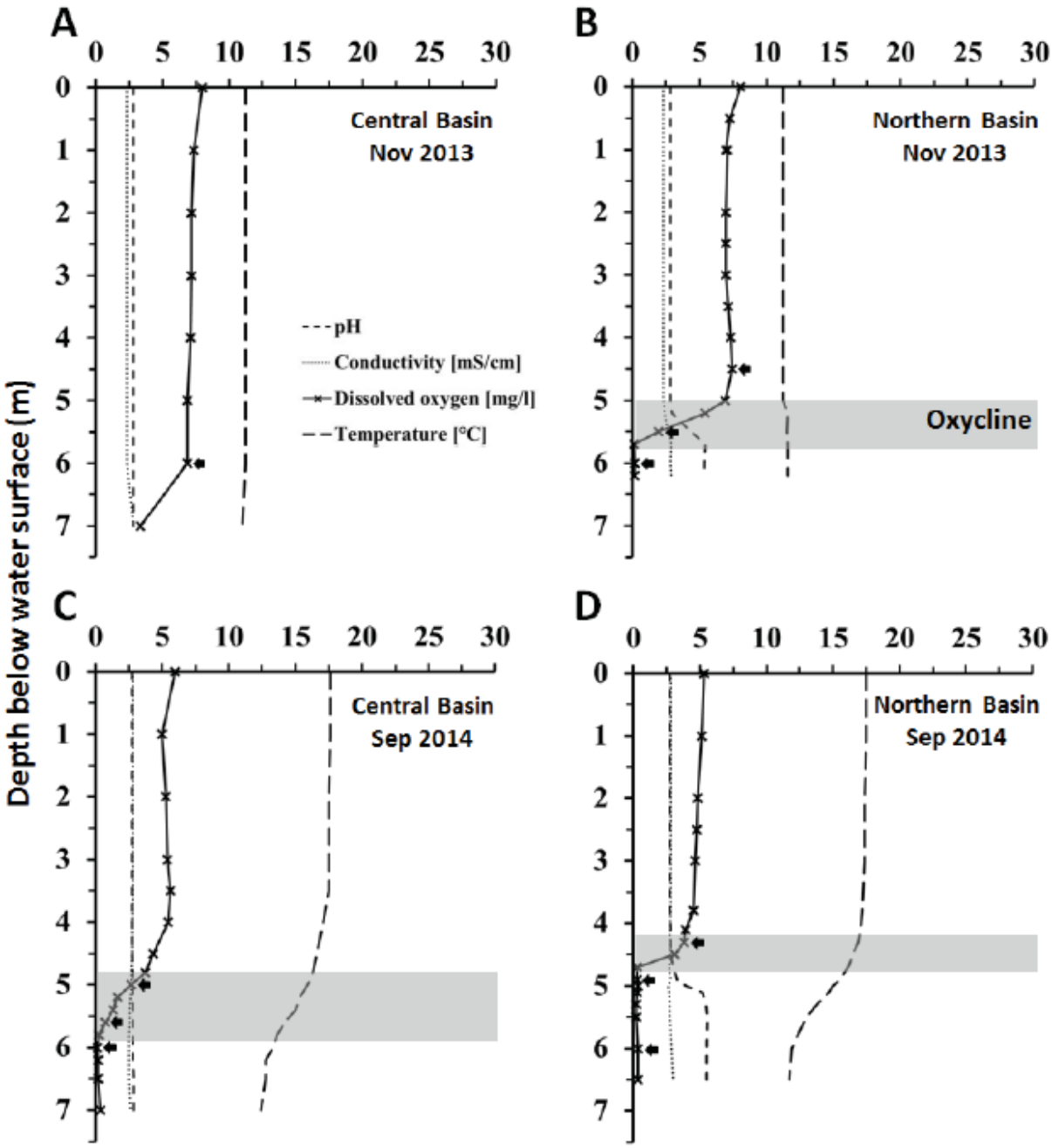

Fig. 1

ACCEPTED MANUSCRIPT

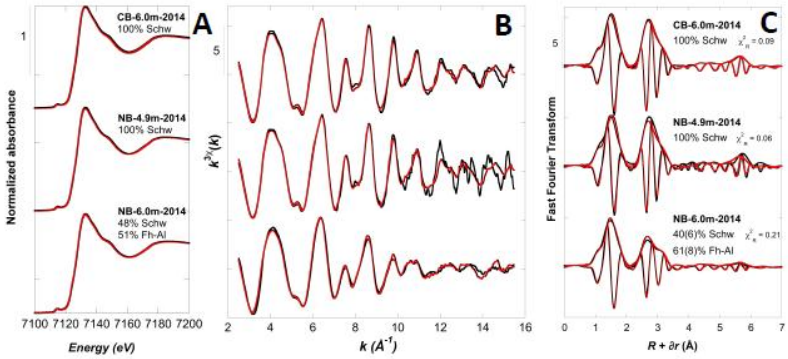

Fig. 2

ACCEPTED

ACCEPTED MANUSCRIPT

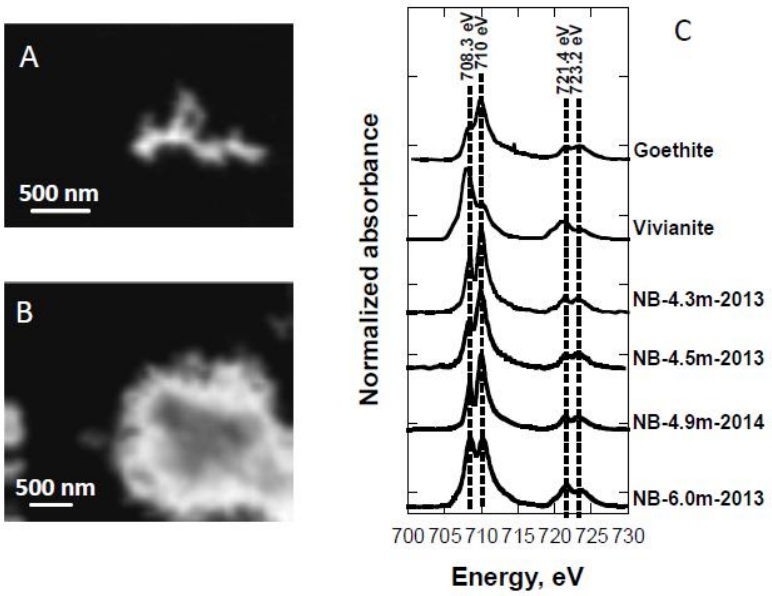

Fig. 3

ACCEPTED

ACCEPTED MANUSCRIPT

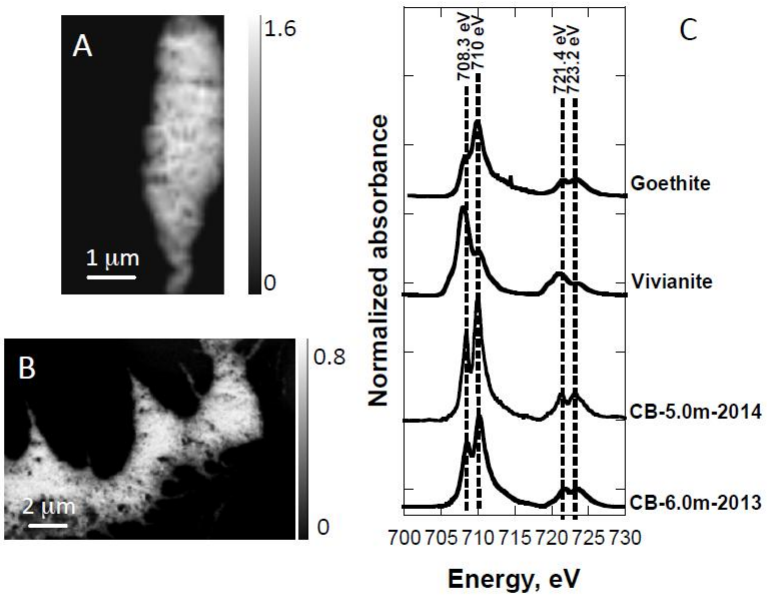

Fig. 4

ACCEPTED

ACCEPTED MANUSCRIPT

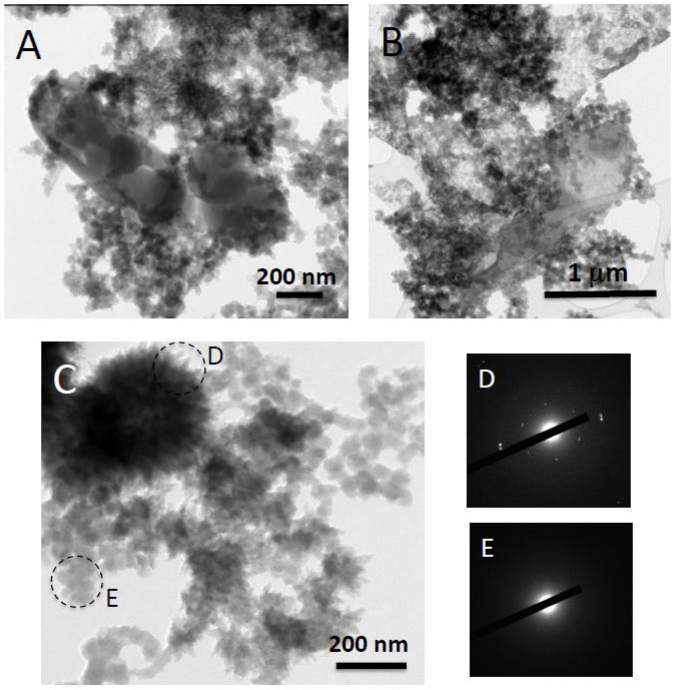

Fig. 5

ACCEPTED

ACCEPTED MANUSCRIPT

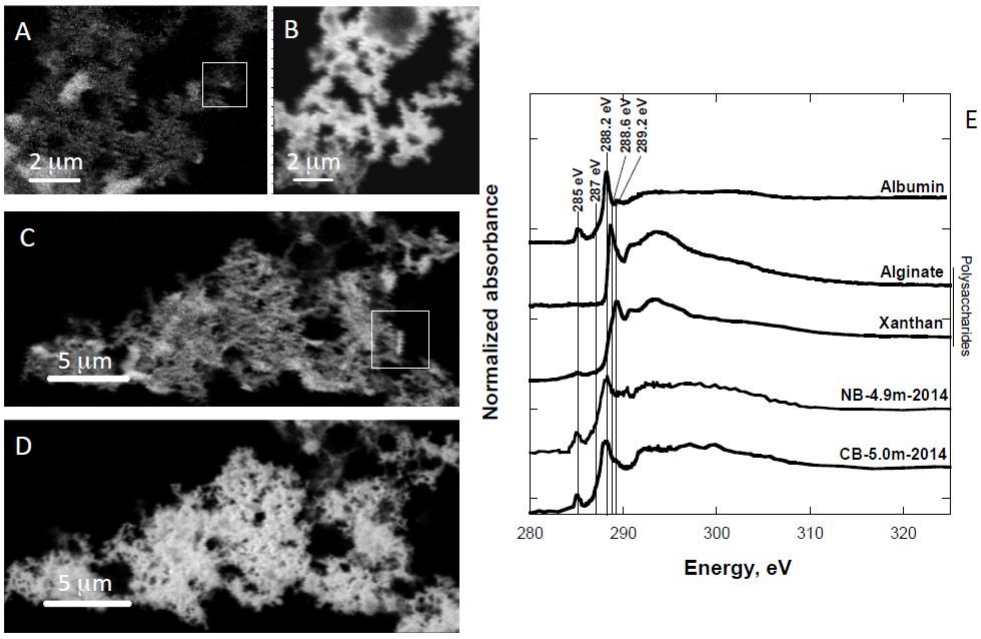

Fig. 6

ACCEPTED

ACCEPTED MANUSCRIPT

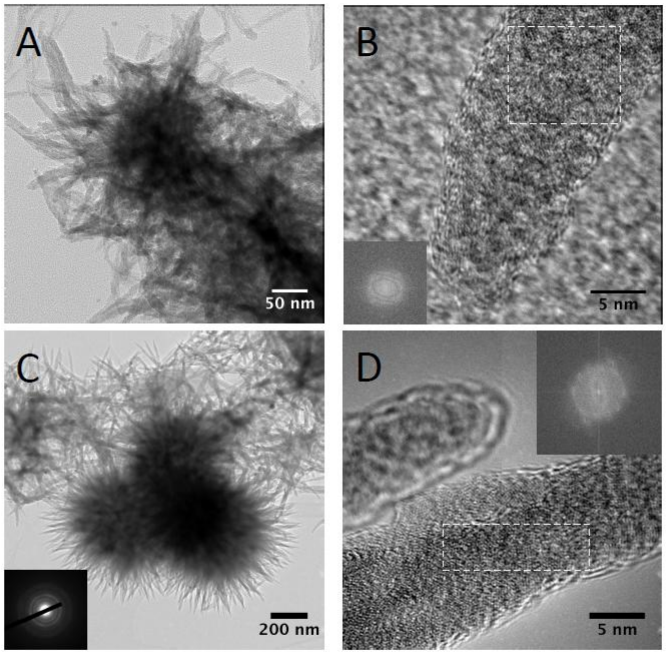

Fig. 7

ACCEPTED

ACCEPTED MANUSCRIPT

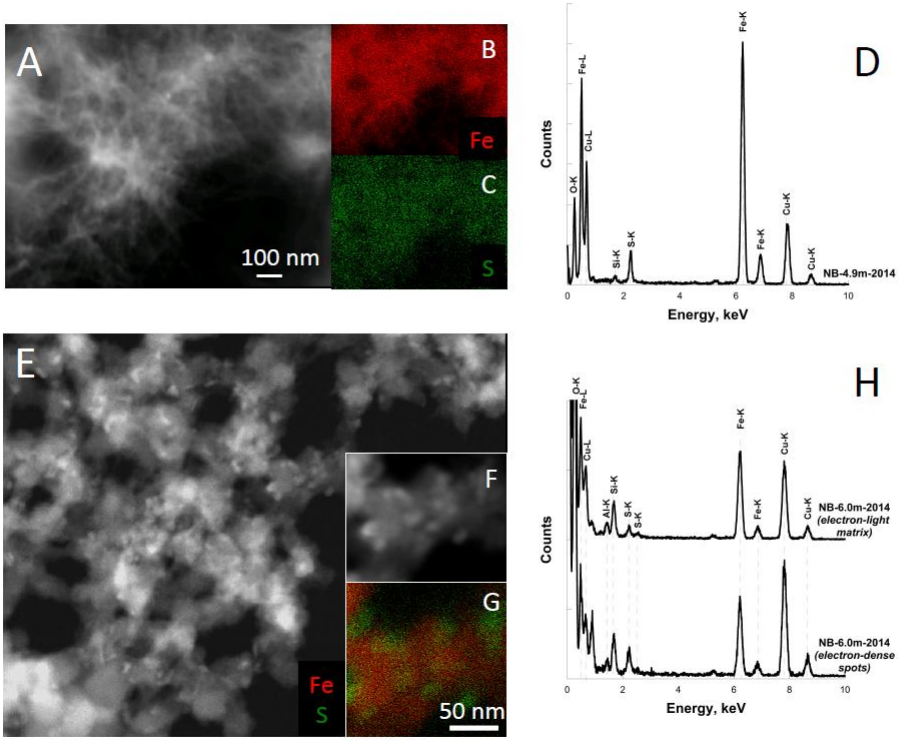

Fig. 8

ACCEPTED

ACCEPTED MANUSCRIPT

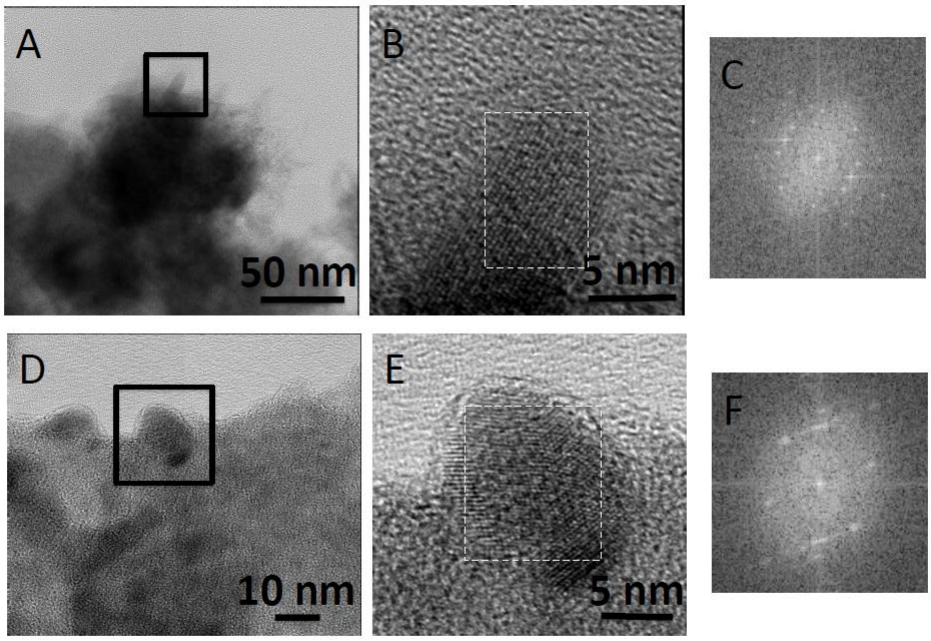

Fig. 9

ACCEPTED

ACCEPTED MANUSCRIPT

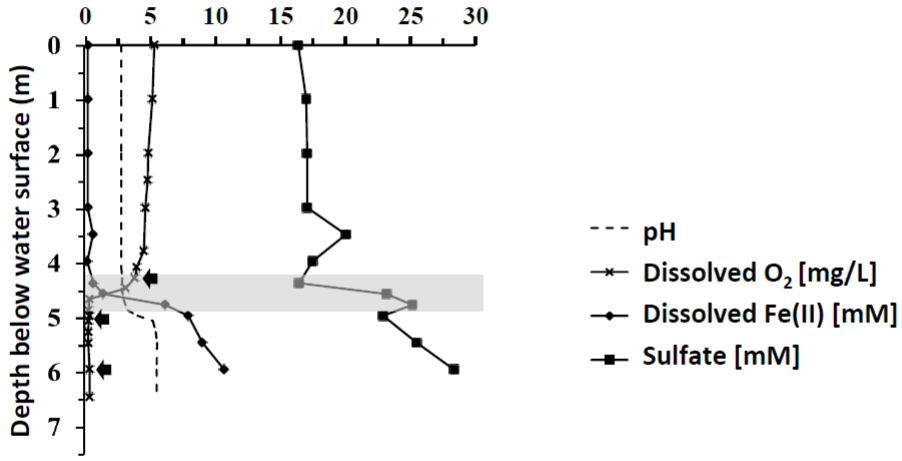

Fig. A1

ACCEPTE

ACCEPTED MANUSCRIPT

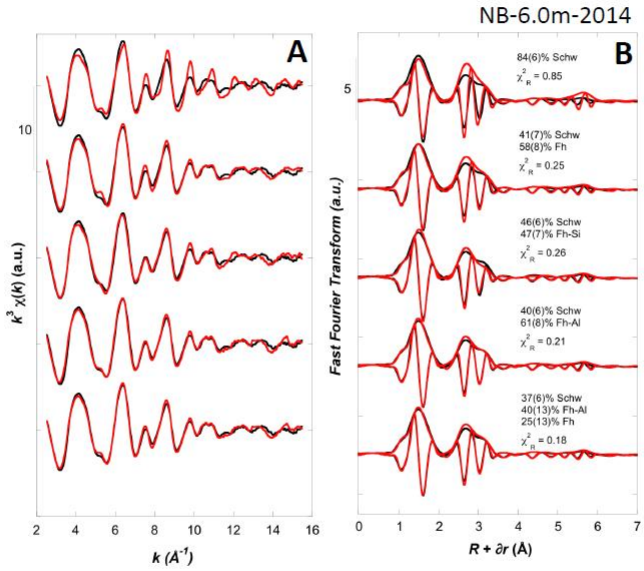

Fig. A2

ACCEPTED

ACCEPTED MANUSCRIPT

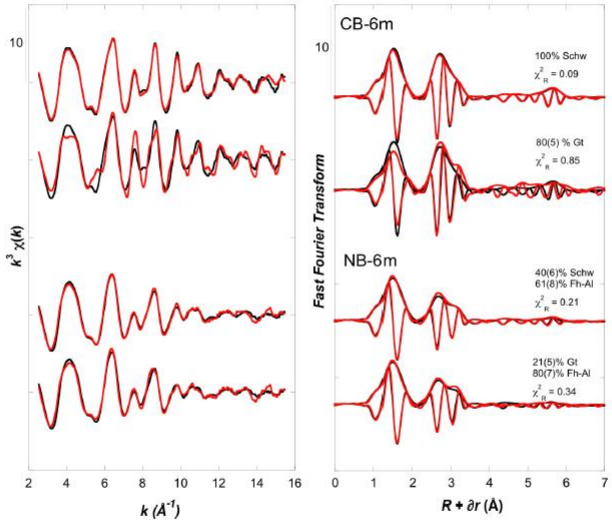

Fig. A3

ACCEPTED

ACCEPTED MANUSCRIPT

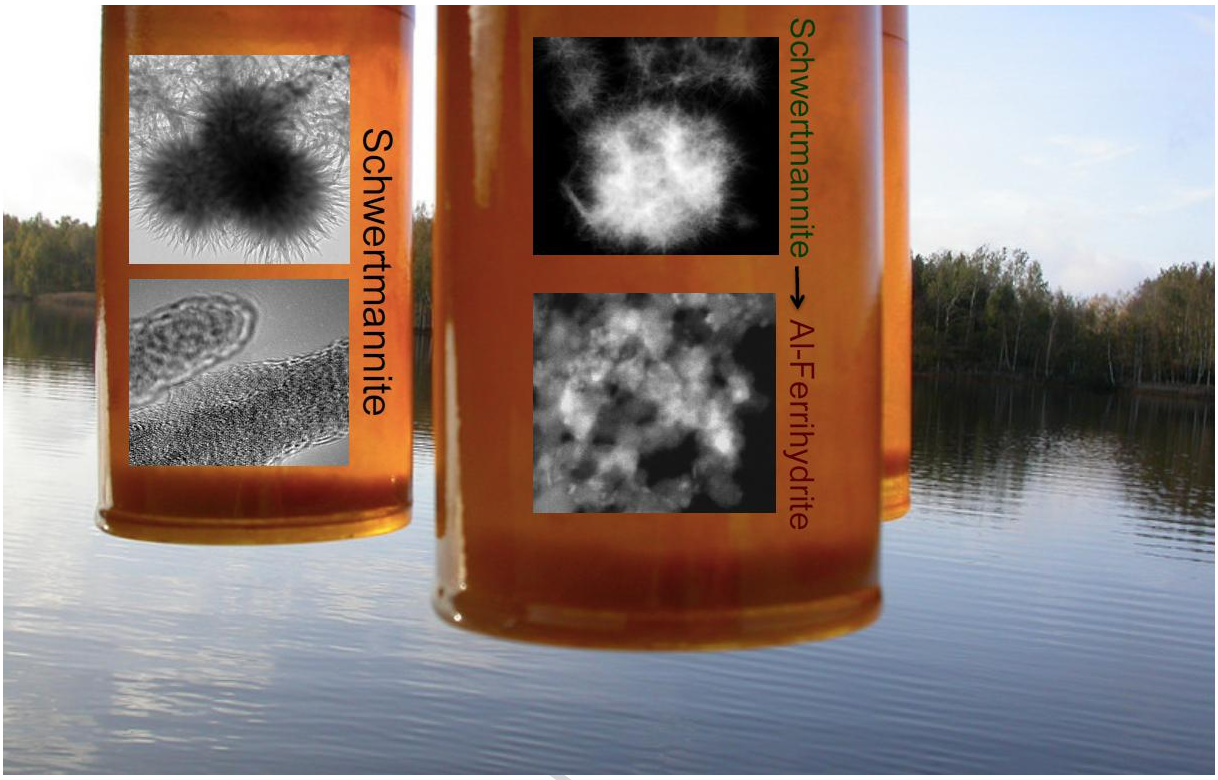

Graphical abstract

ACCEPTED